Economic Geology, v. 108, pp. 1379–1396

The Butte Magmatic-Hydrothermal System: One Fluid Yields All Alteration and Veins

Mark Reed,[1,†] Brian Rusk,[2] and James Palandri[1]

[1] *Department of Geological Sciences, University of Oregon, Eugene, Oregon 97403*

[2] *Department of Geology, Western Washington University, Bellingham, Washington 98225*

Abstract

Mine exposures and deep drilling reveal that the Butte porphyry Cu-Mo ores occur in two, internally zoned domes with alteration assemblages containing biotite, K-feldspar, sericite, and chlorite. A third body of pervasive quartz-sericite-pyrite alteration lies between and overlaps the Cu-Mo–mineralized domes, and has roots that extend to a depth of more than 2 km. The porphyry system is cut by large, throughgoing fissure veins containing copper, zinc, lead, and manganese.

Each of the two Cu-Mo–mineralized domes has concentric zones of widely overlapping shells of centimeter-scale stockwork veinlets. The deepest and innermost zone consists of barren quartz veinlets that grade upward to a thick zone of quartz-molybdenite veinlets that cut veins of the next outward zone, consisting of quartz-sulfide veinlets with biotite-K-feldspar-sericite-andalusite alteration envelopes. The biotite-dominant alteration grades upward to a shell of abundant quartz-magnetite-chalcopyrite-pyrite veins with pale green inner envelopes of sericite-K-feldspar-chlorite bordered by biotite-bearing outer envelopes. Farther upward, the outer envelopes change from biotitic to chloritic, and veins of quartz-pyrite-chalcopyrite with chlorite-sericite-K-feldspar envelopes become abundant, intermixed with pyritic veins with gray sericite and an outer envelope with remnant primary biotite dispersed in sericite-pyrite that has replaced primary feldspars. In the outermost of the concentric shells, biotite crackle veins contain pyrite and epidote, and millimeter-scale veinlets containing sphalerite and galena are bordered by K-feldspar-bearing propylitic alteration. Between the two domes, a zone of intense pervasive sericitic alteration formed around a stockwork of pyrite-quartz veinlets bordered by inner envelopes of gray sericite-pyrite-quartz and an outer selvage of sericitized feldspars and remnant primary biotite.

Geochemical modeling of reaction of a magmatic fluid with Butte granite between 600° and 200°C at 1 kbar shows that the full array of alteration types—from high-temperature biotite-feldspar-andalusite to low-temperature sericite-pyrite-quartz and the main stage advanced argillic and sericitic alteration—could all have formed from a single initial fluid composition as it cooled and reacted with wall rock. The high-temperature model fluid is pH neutral and in equilibrium with biotite, feldspar, and andalusite. It is transformed upon cooling as disproportionation of aqueous SO_2 makes the fluid increasingly acidic. As the acidic fluid is neutralized by rock reaction, it yields all of the observed alteration assemblages in the observed spatial order at the scale of vein envelopes and the scale of the hydrothermal system as a whole. The key implication of this finding is that one single initial magmatic fluid composition is chemically capable of producing all of the alteration and mineralization features observed in the Butte system. Thus, a single fluid composition may form porphyry copper deposits in some settings and shallow epithermal veins in others, or both ore types superimposed in single districts. The universally observed sequence of vein cutting relations in porphyry copper deposits—i.e., high-temperature quartz-chalcopyrite veins with biotite-K-feldspar envelopes cut by moderate-temperature pyrite veins with sericitic alteration, and both of these cut by low-temperature veins containing covellite and enargite with quartz-kaolinite alteration—is likely to be an inevitable consequence of cooling of a single fluid type, not a consequence of successive distinct fluid compositions expelled from an igneous source.

Introduction

The giant porphyry copper deposit in Butte, Montana, is one example of a magmatic-hydrothermal system where an overpressured water-rich magmatic volatile phase hydrofractured overlying granite, then surged through the fractures, forming a stockwork of quartz-sulfide veinlets. Vein cutting relations show that the vein minerals and adjacent alteration envelopes changed mineral content through time, from 650°C early quartz-chalcopyrite with biotite-feldspar alteration to subsequent quartz-molybdenite with little or no alteration, to later pyrite-quartz with intense sericitic alteration and, finally, to main stage throughgoing fissure veins of quartz with base metal sulfides formed at temperatures less than 350°C. Essentially the same vein types and timing relationships are recognized in porphyry copper deposits worldwide (Seedorff et al., 2005; Sillitoe, 2010), reflecting a recurrent fundamental process of magmatic-hydrothermal fluid evolution that is commonly ascribed to evolving magmatic processes controlling fluid character at its source, i.e., the ongoing progress of magma crystallization controls the mix of metals emerging from a magma at any given crystallization stage and those fluid compositions determine the qualities of hydrothermal alteration produced by the fluid (e.g., Candela and Holland, 1986; Cline and Bodnar, 1991; Sillitoe, 2010). In one contrary view, Seedorff and Einaudi (2004a, b) inferred that the transition from potassic to sericitic alteration at the Henderson porphyry Mo deposit was linked to a change in temperature rather than a change in fluid composition. There is also a long-held view that much porphyry copper sericitic alteration reflects meteoric water input, although that concept has been largely overthrown by O and H isotope data from El Salvador (Watanabe and Hedenquist, 2001), Far Southeast (Hedenquist et

† Corresponding author: e-mail, mhreed@uoregon.edu

Submitted: August 24, 2011
Accepted: March 7, 2013

al., 1998), Butte (Zhang, 2000; Rusk et al., 2004), Alumbrera (Harris et al., 2005), Refugio district (Muntean and Einaudi, 2001), the Endeavor 26 North deposit (Harris and Golding, 2002), and Henderson (Seedorff and Einaudi, 2004b). Hedenquist et al. (1998) and Muntean and Einaudi (2001) suggest an influx of multiple magmatic fluids of changing composition to form early potassic and later sericitic alteration, but Seedorff and Einaudi (2004b) conclude that the transition from potassic to sericitic alteration at Henderson was a consequence of a temperature decrease, not a recurrent magmatic fluid pulse, although they do identify recurrent magma pulses.

Measurements of fluid inclusions in the Butte system (Rusk et al., 2004, 2008a, b) show that the salinity and CO_2 concentration of primary fluids are similar in all Butte pre-main stage vein types, suggesting a common origin. Computations of reaction of the fluids with the host Butte granite reported here show that one single fluid composition is capable of yielding veins and alteration of every variety observed. The variations in vein and alteration mineral assemblages result from variations in temperature, from variation in the extent of reaction between fluid and host rock along a flow pathway, and from the effects of pressure drop. In a given deposit, if one fluid type yields all vein stages and alteration types, then the cause of the variations in veins and alteration lies not in magma chamber processes, but entirely in the hydrothermal regime and the staging of its delivery into the fracture system.

In this paper, we introduce the basic features of the Butte alteration assemblages, then focus on thermodynamic computations of wall-rock reactions at 1 kb and a range of temperatures from 600° to 200°C. The models aid in understanding how centimeter-scale zoned alteration assemblages form adjacent to a single vein, and how one alteration assemblage evolves upward to another with decreasing temperature over a scale of many hundreds of meters within the deposit.

Butte Geology

The host rock of the Butte ore deposit is identified as the Butte granite by Emmons and Tower (1897). Sales (1914) used the term "Butte granite" as a matter of custom, even though Weed (1912) called it the Butte quartz monzonite, as have most subsequent workers. However, under the 1974 International Union of Geological Sciences (IUGS) nomenclature (Streckeisen, 1974), it is properly termed "granite" and is so identified here. The Butte granite provides a uniform background rock for study of hydrothermal alteration, which has made Butte an outstanding natural laboratory for study of alteration, exemplified in studies by Sales (1914), Sales and Meyer (1948), Meyer (1965), Meyer et al. (1968), Roberts (1973, 1975), and Brimhall (1977).

The 76 Ma Butte granite constitutes most of the Boulder batholith (Smedes, 1973; Tilling, 1973). It intruded Proterozoic sedimentary rocks of the Belt Supergroup and, to the south of Butte, Archean crystalline basement. The granite is medium to coarse grained, containing nearly equal amounts of quartz and K-feldspar, together totaling 40 to 45 vol %. Plagioclase constitutes 36 to 40 vol %, and biotite, hornblende, and accessory magnetite, sphene, ilmenite, and apatite make up the remaining 15 to 20 vol % of the pluton (Meyer et al., 1968; Roberts, 1975). The Butte granite is cut by dikes and subhorizontal sheets of aplite that constitute a small volume of the host rock, but locally host intense vein stockworks.

The overview of Butte porphyry copper veins and alteration given here is based on mapping drill core from 10 deep surface diamond drill holes drilled in the late 1970s and early 1980s, plus mapping of underground crosscuts and drill holes driven and drilled in the same time interval in the Kelley, Steward, and Leonard mines (Fig. 1) on the 2,000-, 3,400-, 4,200-, and 4,600-foot mine levels (Fig. 2). Details of spatial distribution of alteration and its mineralogy and composition are the subject of a separate contribution. Our purpose here is to outline the basic alteration mineralogy and its gradational changes with depth to provide a basis for examination of how reaction of a magmatic fluid with the host granite at a range of temperatures may produce the observed alteration.

Butte vein and alteration terms

Vein "types," per se, are classified by whatever provides conspicuous uniquely distinguishing features, whether it is vein mineral content, alteration envelope assemblages, or structural style. In Butte, Early Dark Micaceous (EDM) (Meyer, 1965), Pale Green Sericitic (PGS), Dark Green Sericitic (DGS), and Gray Sericitic (GS) veins are distinguished by alteration envelope minerals (Table 1). In contrast, quartz-molybdenite and barren quartz veins mostly lack alteration and are distinguished by vein minerals. The late, large, throughgoing fissure-filling veins of the main stage are distinguished by structural character (Meyer et al., 1968). The alteration terms—EDM, PGS, DGS, GS, and Sericite with remnant granite biotite (SBr)—are petrologic rock names referring to specific mineral assemblages as explained below and laid out in Table 1.

Butte mineral zones, veinlets, and alteration

The Butte copper and molybdenum mineralization lies in two domes that are 1 to 2 km in diameter (Figs. 1, 2) and that straddle a quartz porphyry dike swarm. The term "dome" reflects the squat hemispherical shape, and is adopted from "moly dome," the term used informally by Charles Meyer to refer to the molybdenite zone described by Meyer et al. (1968). Between the two Cu-Mo domes lies a well-defined body of pervasively sericitized rock (Figs. 1, 3). The Anaconda and Pittsmont domes are composed internally of widely overlapping concentric shells of millimeter- to centimeter-scale stockwork veinlets (Figs. 2, 3). The deepest are barren quartz (Fig. 4a) and quartz-molybdenite (Fig. 5a) veins that cut and overlap a gradational series of veins that change outward from quartz-chalcopyrite dominant to quartz-chalcopyrite-magnetite-pyrite, to pyrite-quartz (Figs. 4, 5). Their alteration envelopes change from deep biotite-K-feldspar-sericite to chlorite-K-feldspar-sericite and sericite-pyrite alteration in the shallow setting.

Barren quartz and quartz-molybdenite: The deepest veins, explored in the deep reaches of drill holes exceeding 1,700 m (Fig. 3), are barren quartz (Fig. 5f). The barren quartz stockwork has been intersected in the geometric center of the district (Fig. 3), but is also intersected beneath the center of the Pittsmont dome in the bottom 100 m of drill hole 2, in the footwall of the Continental fault (Fig. 1). Accounting for the fault displacement, the deep Pittsmont barren quartz

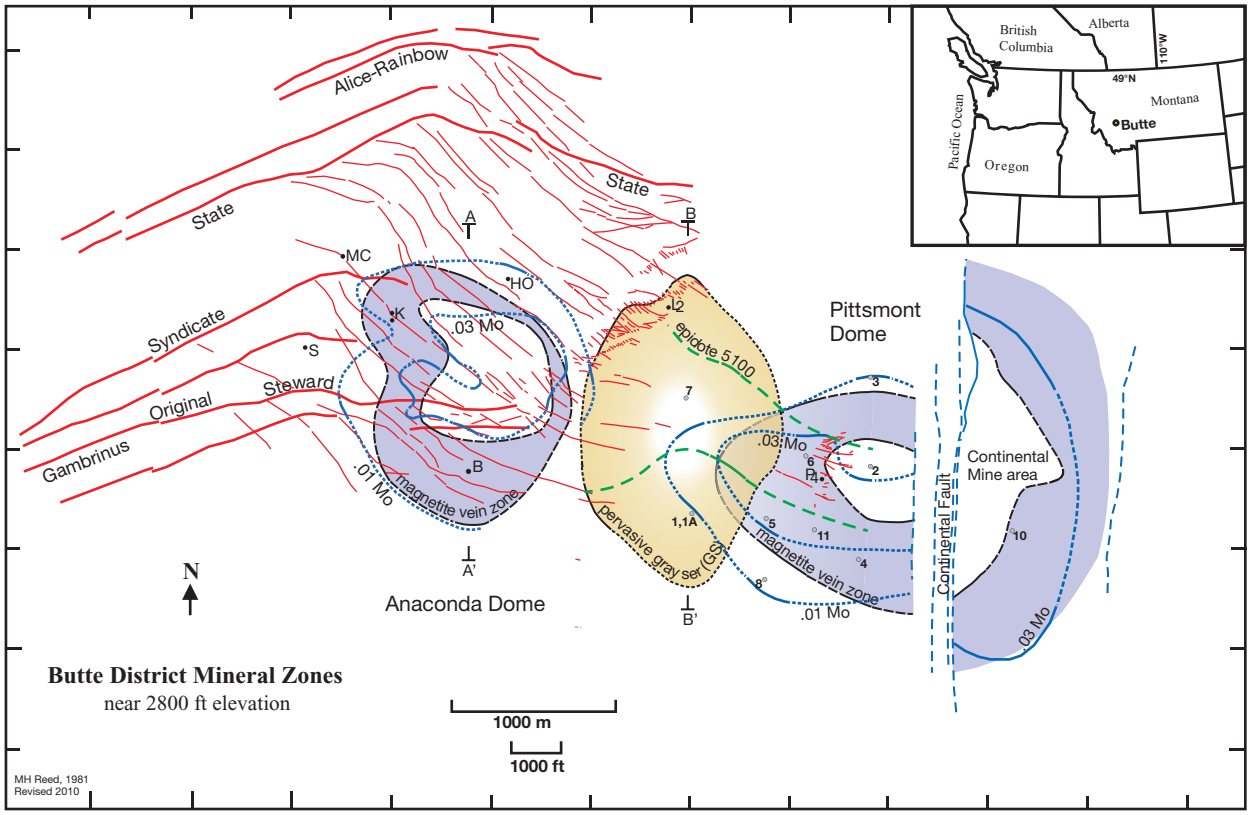

FIG. 1. Butte district mineral centers and main stage veins, 2,800-ft elevation. Mine shafts: B, Belmont; HO, High Ore; K, Kelley; L2, Leonard #2; MC, Mountain Consolidated; P4, Pittsmont; S, Steward. Small circles with numbers in the eastern half of the map area identify deep drill holes. Green lines define the inner limit of epidote at 5,100-ft elevation. Blue contours show Mo grade in wt %, dashed where interpolated or projected. The red lines show the main stage veins, including the Leonard horsetails, which refers to the short, closely spaced veins near the Leonard shaft. The horsetail veins contain the high-sulfur assemblage, pyrite, enargite, covellite, and digenite, and are bordered by advanced argillic alteration. A-A' and B-B' identify the locations of the cross sections shown in Figures 2 and 3.

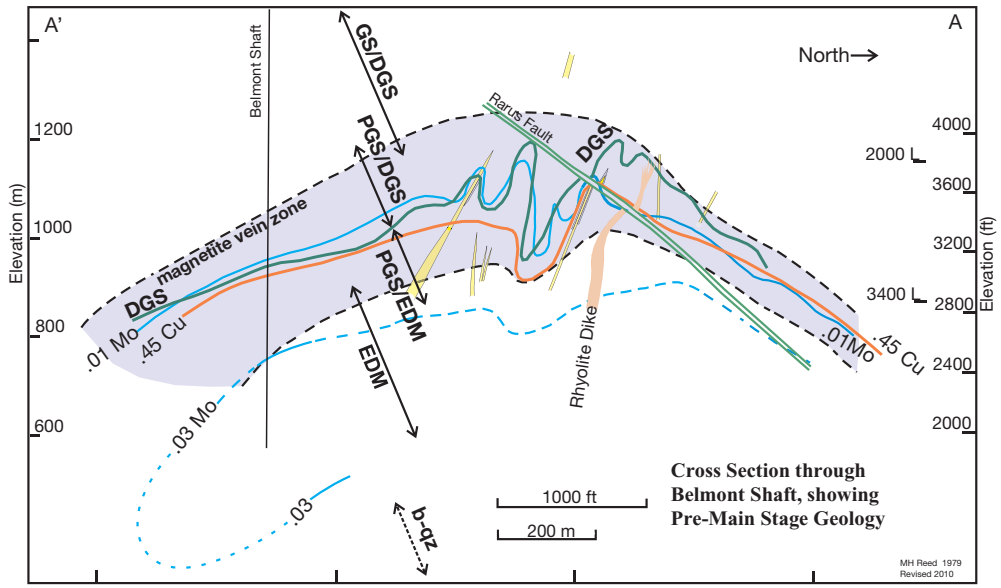

FIG. 2. North-south cross section through the Anaconda dome, Butte district, along section line A-A' of Figure 1. Blue contours show Mo grade in wt %, dashed where interpolated or projected. Yellow identifies quartz porphyry dikes. Dark green sericite-chlorite alteration occurs above the green curve labeled DGS. The arrows labeled with EDM, PGS/EDM, PGS/DGS, and DGS/GS identify the concentric gradational series of veinlet alteration zones (see Table 1 for alteration terms). The barren quartz (b-qz) vein zone is projected to this section based on data in deep drilling to the east.

Table 1. Alteration Types

Alteration type; zone	Defining minerals and textures; alteration mineral reactions: [granite mineral] > alteration mineral	Metallic minerals in veins & alteration
Early Dark Mica (EDM); beneath and lapping into mt vein zone	Brown & green shreddy biotite; kf rims musc [plag] > musc, kf, shreddy bi, plag: ab(94–98), an(23–30) ± and ± cor, anh, carb [kf] > musc, kf: or(93), bi [hornb] > bi, anh, kf [bi] > bi (re-xl, increased Mg/Fe)	cp, py ± mt mb (veins only)
Pale Green Sericitic (PGS); mt vein zone -PGSk includes kf -PGSs lacks kf, chl	Pale green musc, kf, & fine chl; granite texture destroyed [plag, kf] > musc ± kf, qz, chl⁻ (ser island txt) [bi, hornb] > musc, chl, carb	cp, py, mt
Dark Green Sericitic (DGS); upper mt zone and above	Dark green chlorite; granite texture intact [plag] > pale green musc ± kf, qz, chl [kf] > musc ± kf, qz [bi] > chl unit pseudomorph, rt grid	cp, py ± mt
Propylitic (Pr); peripheral	ep, chl; granite texture intact [plag] > ser, ep, chl, kf [kf] > largely fresh [bi] > chl, py [hornb] > ep, chl, py	sl, gn, cp, py ± rc
Gray Sericitic (GS); exterior to mt zone, central QSP zone	gray qz, ser, pyrite; texture destroyed [plag, kf] > qz, musc, py [bi, hornb] > musc, py, qz, Mg chl, rt	py, cp
Sericitic with remnant biotite (SBr); exterior to mt zone; central QSP zone	Texture mostly destroyed [plag, kf] > qz, musc, py [bi] > remnant bi (increased Mg/Fe), musc, py	py, cp

Mineral abbreviations: ab = albite, an = anorthite, and = andalusite, anh = anhydrite, bi = biotite, carb = carbonate, chl = chlorite, cor = corundum, cp = chalcopyrite, ep = epidote, gn = galena, hornb = hornblende, kf = K-feldspar, mb = molybdenite, mt = magnetite, musc = muscovite, plag = plagioclase, py = pyrite, QSP = quartz-sericite-pyrite, qz = quartz, rc = rhodochrosite, re-xl = recrystallized, rt = rutile, ser = sericite, sl = sphalerite, txt = texture

stockwork is 2,600 m beneath the surface, placing it about 1,000 m below sea level elevation. With reference to Figure 3, that 1,000 m below sea level elevation indicates a vertical extent of quartz stockwork of at least 1,000 m.

As density of the stockwork thins upward, some quartz veins grade into quartz-molybdenite veins with no obvious change in vein or alteration mineral content, with the exception of molybdenite abundance (Fig. 5a). These veins reach high into the Pittsmont and Anaconda domes, extending conspicuously, for example, to the 0.01% Mo grade contour (Figs. 1–3). The deepest of the quartz-molybdenite veins in the Pittsmont dome have narrow biotitic or K-feldspar alteration envelopes, but shallower examples lack alteration.

EDM: The quartz-molybdenite veins cut and overlap upward veins of the potassic series, consisting of veins with biotite-K-feldspar alteration at depth that change gradationally upward through a series of alteration assemblages ending in propylitic alteration, nearly all of which include added K-feldspar in part of the vein envelope. The deepest of the potassic series are quartz-chalcopyrite-pyrite veins with biotite-K-feldspar-sericite ± andalusite alteration (Fig. 4d) designated "EDM" by Meyer (1965), and further described by Roberts (1975) and Brimhall (1977). The earliest Butte veinlets are a variant of EDM alteration called "biotite crackles," consisting of biotite-altered wall rock along planar cracks, some of which emanate directly from biotite breccias (Fig. 4a), which form at the leading edges of quartz porphyry dikes. Biotite breccia consists of sand-sized to centimeter-scale rotated angular to subrounded fragments of granite and aplite suspended in a dark matrix of biotite, quartz, K-feldspar, chalcopyrite, and pyrite (Brimhall, 1977). The direct physical connection of biotitic alteration to biotite breccia and the breccia to porphyry indicates that the hydrothermal fluids that formed the potassic mineral assemblage of EDM alteration emerged from magma.

EDM alteration has complex textures, as demonstrated in Figure 6, which shows an EDM assemblage of biotite, K-feldspar (Or90), quartz, muscovite, andalusite, albite (Ab94-99), plagioclase (An23-30), anhydrite, and corundum. As Roberts (1975) documented, this EDM plagioclase is newly precipitated and distinct from the An40 granite plagioclase. These coexisting albite and oligoclase compositions, determined by electron microprobe analysis, reflect the peristerite gap in plagioclase solid solutions, and some of the albite fringing textures visible in Figure 6 probably form by plagioclase unmixing across the peristerite gap. The equilibrium of andalusite with muscovite, K-feldspar, and quartz indicates a temperature of 600°C at 2 kb pressure (Spear, 1993), which is consistent with temperatures determined for EDM and quartz-molybdenite veins by Mercer and Reed (2013) from concentrations of Zr in rutile, Ti in biotite, and Ti in quartz. At shallower depths, EDM alteration lacks andalusite and An26-plagioclase while keeping its distinctive biotite, plus muscovite and K-feldspar.

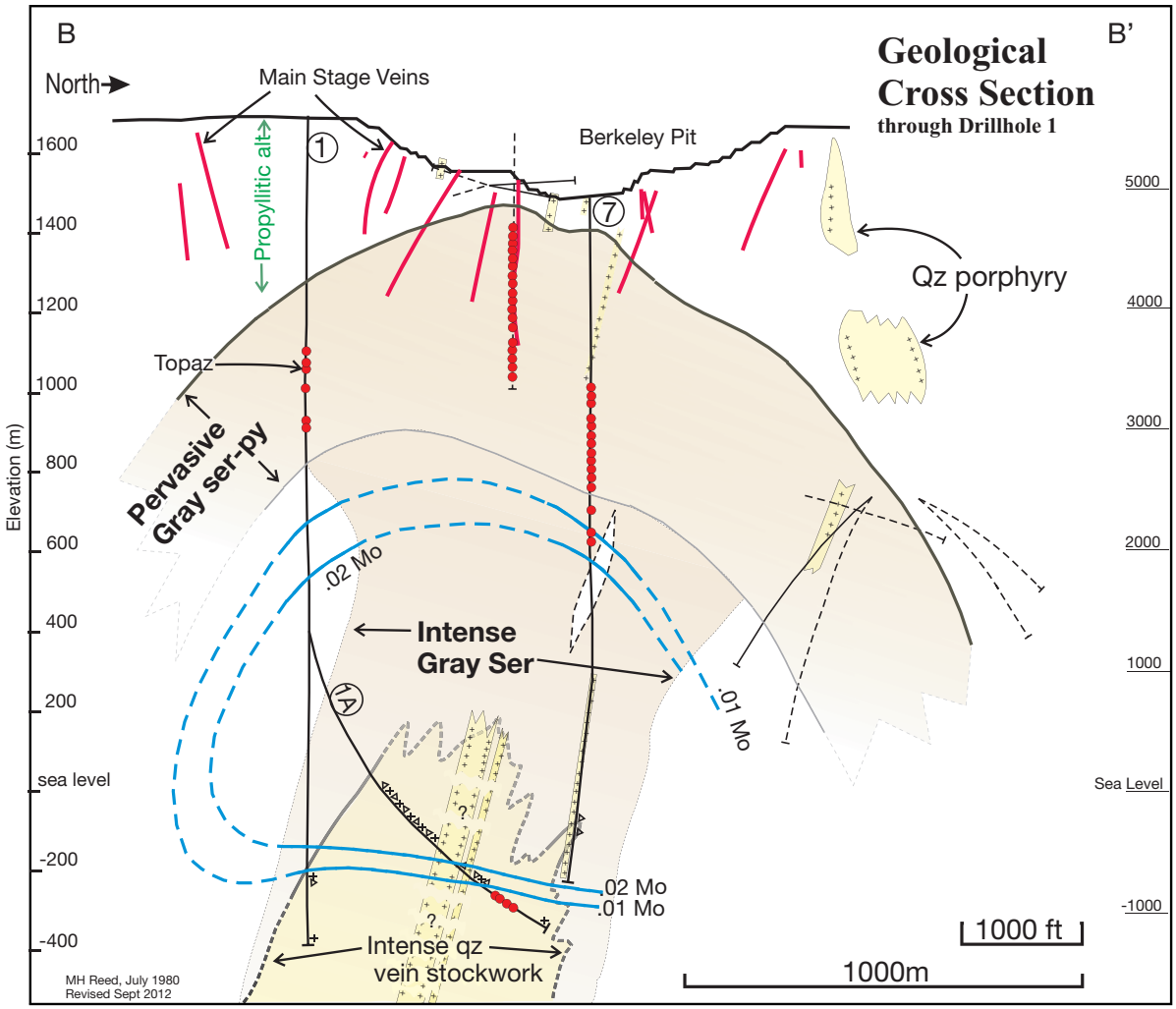

FIG. 3. North-south cross section through the Butte district deep drill holes 1, 1A, and 7 (circled numbers) along section line B-B' of Figure 1. Light brown shading shows Gray Sericitic (GS) alteration, which occurs in a mushroom-shaped zone with a cap of pervasive GS alteration with very abundant pyrite (>6 wt % bulk Fe) and a stem of intense GS alteration, but much less pyrite (<3.5 wt % bulk Fe). At depth in the three deep drill holes in this cross section (and deep in drill hole 2, Figure 1) is a zone of intense quartz stockwork veining, wherein all original rock is intensely altered to GS with subordinate SBr. Main stage veins (red), explored and partially mined, occur above and partway down into the GS zone. Along some of those veins and elsewhere within the GS zone, the rock is altered to topaz (red circles) and the adjacent veins typically contain enargite, covellite, and pyrite. The molybdenite vein zone of the Pittsmont dome (Fig. 1) is displayed in this section by blue contours showing Mo grade in wt %, dashed where interpolated or projected. Yellow with "+" symbols identifies quartz porphyry, of which the northernmost three occurrences are the younger Modoc porphyry plug. The scattering of "+" and "Δ" symbols along drill hole traces, especially hole 1A, indicates mixed quartz porphyry, breccia, and granite on a scale of 1- to 2-m drill hole lengths. Surface and underground drill holes are shown with dashed lines where they are projected to the section plane and solid lines where they are in the plane. These holes, mine workings, and gravity measurements were used to constrain the edges of the GS zone and other geologic features in this section.

PGS, DGS, and the magnetite vein zone: EDM veins grade upward to quartz-chalcopyrite-pyrite-magnetite veins bordered by pale green sericite-K-feldspar-chlorite alteration (PGS) with an EDM outermost halo (quartz-chalcopyrite-pyrite-magnetite//PGS/EDM; Fig. 4c, e, f; note that vein and alteration halo minerals are abbreviated here with a double slash separating vein minerals from alteration and a single slash separating alteration zones within the vein envelope; Seedorff and Einaudi, 2004a). PGS alteration lacks shreddy biotite and andalusite, but otherwise resembles EDM alteration in containing K-feldspar and sericite replacing granite feldspars. The vein magnetite in many of the magnetite-bearing PGS/EDM veins occurs in distinctive masses (e.g., Fig. 4f) such that the veins are readily mapped in drill core and crosscuts, enabling a straightforward tracking of the magnetite vein zone shown in Figures 1 and 2, the inner edge of which is sharp, but the outer edge in the PGS/DGS vein zone (see below) is diffuse.

Partway outward through the magnetite vein zone, the outer EDM halo of the PGS/EDM veins is displaced by a halo of dark green chlorite-sericite-K-feldspar, DGS, which is distinguished by the replacement of primary rock biotite by unit pseudomorphs of chlorite, and by the absence of shreddy biotite (Fig. 5e). DGS alteration otherwise includes sericite,

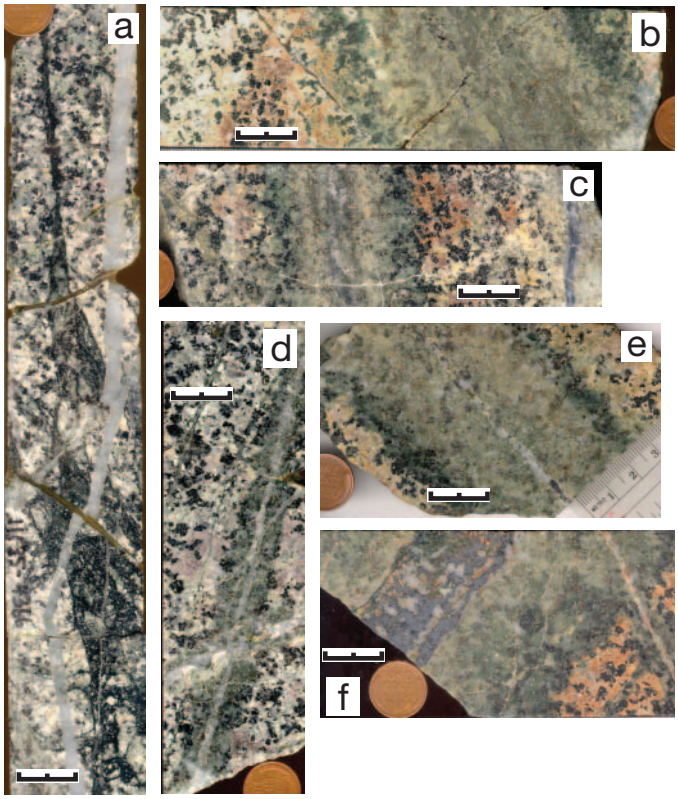

FIG. 4. Polished slabs of Butte veins illustrating alteration and vein types. Scale bar is 20 mm; coin is 19 mm in diameter; all images are at the same scale. See Table 1 for definitions of alteration terms used in the following descriptions. a) Biotite breccia bleeding upward into biotite crackle veinlets, cut by 4- to 8-mm barren quartz veinlet (11135-4366, deep in center of Pittsmont dome). b) Pyrite-quartz vein bordered by zoned GS/DGS alteration envelope, surrounded by late argillic alteration (10854-1261, 2,000 level, center of Anaconda dome). c) Quartz-pyrite-chalcopyrite-magnetite vein with PGS/EDM envelope; 3-mm quartz-molybdenite veinlet and separate pyrite vein at right end (11135-2187, center of Pittsmont dome). d) 2-mm quartz-chalcopyrite-pyrite-molybdenite vein with prominent EDM envelope and parallel biotite crackles to its left, cut by quartz-pyrite-chalcopyrite vein with weak PGS alteration (11135-3618, center of Pittsmont dome). e) Quartz-pyrite-chalcopyrite-magnetite vein with PGS/EDM alteration, surrounded by later argillic alteration (10778-6, 3,400 level of northwest Anaconda dome). f) 27-mm quartz-magnetite-pyrite-chalcopyrite vein with PGS/EDM envelope, illustrating abundant magnetite that is characteristic of much of the magnetite zones shown in Figures 1 and 2 (10961-766, north flank Anaconda dome, 3,200-ft elevation).

chlorite, and K-feldspar replacing feldspars and is distinctive for its dark green color, making it easy to map, as shown by the DGS contour in Figure 2.

Gray sericitic alteration, peripheral pyritic veins, and propylitic alteration: Toward the periphery of the magnetite zone, the PGS veins become distinctly pyritic and less green, and thereby grade into "Gray Sericitic" alteration (sericite-pyrite with colorless Mg chlorite and no K-feldspar), which forms veinward envelopes in GS/DGS veins (Figs. 4b, 5d). In many cases, the veinward PGS or GS alteration is absent, yielding quartz-pyrite-chalcopyrite//DGS veins (Fig. 5e), wherein the DGS alteration is intense, including prominent secondary K-feldspar with sericite and chlorite replacing plagioclase. The DGS alteration in some distal GS/DGS envelopes lacks K-feldspar, but retains sericite and green Fe chlorite.

A second peripheral vein type overlapping and extending upward beyond the DGS vein zone consists of crackles and millimeter-scale veinlets of quartz-chalcopyrite-sphalerite-galena ± rhodochrosite ± chlorite ± epidote with propylitic alteration, wherein the propylitic alteration consists of epidote, sericite, chlorite, carbonate, and K-feldspar. Propylitic alteration also occurs where epidote augments the outer edges of some distal DGS vein envelopes. Propylitic alteration occurs outboard from the epidote contour shown in Figure 1, which was mapped in Berkeley pit drill holes by Page (1979), and subsequently extended eastward from deep drilling.

Between the Anaconda and Pittsmont domes (Fig. 1) and extending to great depth in the shape of a mushroom with a fat stem (Fig. 3) lies a stockwork of pyrite-quartz veins with intense GS alteration that cuts other vein types (Fig. 5c), except the main stage (Fig. 5b). Where the latter veins are widely enough spaced, an outer envelope is visible where sericite replaces feldspars but primary rock biotite remains (SBr; Fig. 5c). GS alteration of the central mushroom zone contains the same minerals and destroyed texture as the GS alteration of GS/DGS veins described above, but the central mushroom GS veins cut quartz molybdenite veins nearly universally, placing these GS veins later than nearly all molybdenite veins, in contrast to the potassic series veins, which are earlier than molybdenite. There are also GS/SBr veins in the periphery of the Anaconda and Pittsmont domes (as opposed to the central mushroom zone) that precede GS/DGS veins in single locations (e.g., Fig. 5d).

In summary, there are two common variants of pyritic veins with GS alteration in the periphery of the Anaconda and Pittsmont domes, one with GS/DGS envelopes that lie at the distal end of the gradation in the potassic series, and the second with GS/SBr envelopes, for which the relationship to the potassic series is unclear. In the central GS mushroom-shaped zone (Fig. 3), only GS/SBr envelopes occur.

Main stage veins: Large, throughgoing veins of the main stage (Figs. 1, 3) cut all of the veinlets of the potassic series, quartz, and quartz-molybdenite, and the GS types (e.g., Fig. 5b). Main stage veins are bordered by inner sericitic and outer kaolinite-smectite alteration—the "intermediate argillic" of Meyer and Hemley (1967), but the smectite alteration formed only where the main stage fluids encountered granite with fresh plagioclase. A hit-or-miss late main stage overwash argillized fresh granite plagioclase outboard of some EDM and DGS envelopes, as shown in Figures 4b to f and 5d.

In the Leonard Horsetail zone (Fig. 1) and in veins that traverse the central zone of intense GS alteration (Fig. 3), most main stage veins contain pyrite, covellite, and enargite ± digenite ± chalcocite, and are bordered by advanced argillic alteration (Meyer et al., 1968) consisting of innermost quartz accompanied outward by kaolinite/dickite, pyrophyllite, and fluorescent topaz. The advanced argillic envelope is surrounded by white sericitic alteration.

Vein stages: Cutting relations among the vein types outlined above show that four vein stages can be distinguished. The earliest veins are the whole series from deep to shallow, spanning biotite crackles and EDM, PGS/EDM, GS/DGS, DGS, and propylitic alteration. These are veins of the "potassic series," which are cut by quartz-molybdenite veins. The quartz-molybdenite veins are cut by GS alteration (and GS/SBr) in

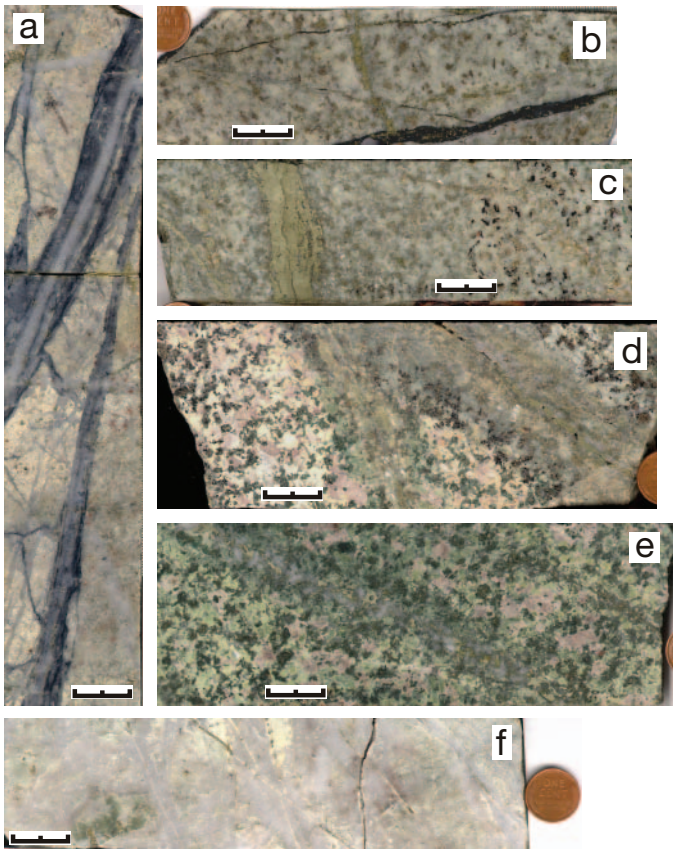

FIG. 5. Polished slabs of Butte veins illustrating alteration and vein types. Scale bar is 20 mm; coin is 19 mm in diameter; all images are at the same scale. See Table 1 for definitions of alteration terms used in the following descriptions. a) Wide, banded quartz-molybdenite veins cutting small barren quartz vein stockwork, all in aplite dike within the Butte granite (10969-5699, deep in southwest flank of Pittsmont dome). b) Intensely GS altered granite with prominent pyrite replacement of biotite; main stage 3- to 8-mm enargite-pyrite vein cuts pyrite-quartz vein (11170-895, center of central GS zone). c) Pyrite vein with GS/SBr envelope (10969-1410, south flank of central GS zone). d) Pyrite-quartz vein (right) with GS/SBr alteration, and pyrite-quartz vein (left) with GS/DGS alteration. The GS/SBr vein preceded the GS/DGS vein in this sample (10759-601, north flank Anaconda dome, 2,000 level). e) 8-mm quartz-pyrite-chalcopyrite vein with DGS alteration and an outer envelope of DGS alteration with remnant primary K-feldspar (pink) (10854-27, central Anaconda dome, 2,000 level). f) Quartz vein stockwork in intensely sericitized aplite, dusted with fine-grained pyrite and cut by millimeter-scale veinlets of quartz and pyrite with minor sericite (11052-7323, near the end of drill hole 1A, Fig. 3).

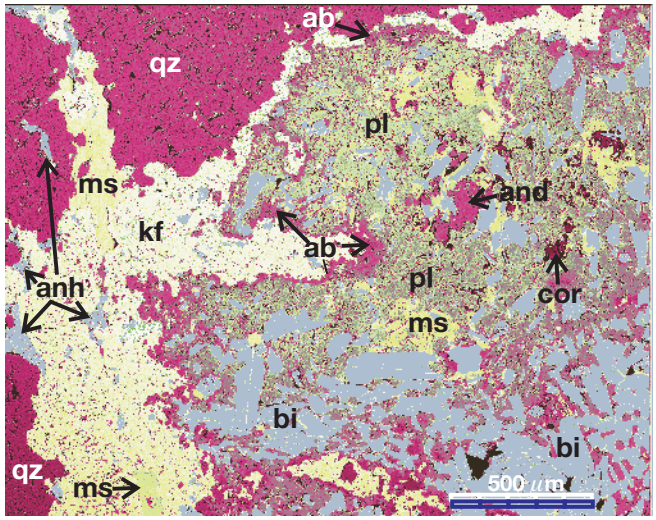

FIG. 6. False-colored backscattered electron-scanning electron microscope image showing EDM alteration (Table 1) bordering a barren quartz vein (far left and upper left). Vein quartz and Butte granite quartz in the alteration envelope is separated from other minerals by K-feldspar. A thin layer of albite separates K-feldspar from plagioclase and biotite. Andalusite and traces of corundum, both with muscovite, occur in the plagioclase-dominated field (11172-2756). Abbreviations: ab = albite, and = andalusite, anh = anhydrite, bi = biotite, cor = corundum, kf = K-feldspar, ms = muscovite, pl = plagioclase, qz = quartz.

the central zone of intense GS alteration (Fig. 1), although, rarely, the reverse is observed. Main stage veins cut all other types. We also find that veins of the potassic series cut others in the series in a retrograde sense, i.e., shallower cuts deeper, e.g., DGS cuts EDM.

Fluid Inclusion Evidence for a Single Primary Fluid

Fluid inclusion studies (Rusk et al., 2004, 2008a, b) suggest that fluids that formed all of the vein types at Butte were derived from a magmatic source and the magma-derived fluid maintained relatively constant bulk composition throughout the evolution of the hydrothermal system, aside from phase separation at low pressure. The evolution of this single parental fluid can yield all of the observed fluid inclusion types (Rusk et al., 2008a) and, as explained below, the single parental fluid could plausibly have formed all of the vein types observed at Butte by its varied paths of cooling, depressurization, and wall-rock reaction.

The deepest and earliest veins at Butte—quartz-rich and sulfide-poor EDM veins—trapped B35 fluid inclusions near 600°C and 2 kb ("B35" and analogous notation below refers to fluid inclusions with 35 vol % vapor bubble, as explained by Rusk et al., 2008a). The B35 inclusions contain 2 to 5 wt % NaCl equiv, 2 to 10 mol % CO_2, and copper and iron in the range of thousands of ppm. B60 fluids in the latest pre-main stage veins (GS veins) also contain 2 to 5 wt % NaCl, and 2 to 10 mol % CO_2, but microthermometry measurements show that these veins formed at temperatures of about 400°C and pressures in the range of 600 bars. Rusk et al. (2008a) argue that the B60 fluids formed by cooling and depressurizing the B35 fluids at pressures and temperatures above the solvus, where unmixing of B35 fluids did not occur.

Unmixing of B35 fluids did occur at moderate depths, forming the B85 vapors and B15H brines, which are halite saturated at room temperature. Where unmixing occurred before significant cooling, some saline fluids formed EDM veins, followed by further cooling to form PGS and some GS veins. The largest proportion of B15h (brine) inclusions occurs in magnetite and chalcopyrite-rich EDM and PGS veins, reflecting depressuring of the B35 fluid at moderately high temperature.

Main stage fluids (Rusk et al., 2008b) are also low salinity (<5 wt % NaCl equiv) and contain a small amount of CO_2 (<3 mol %). These fluids were trapped at temperatures between 250 and 350°C at pressures that are largely unconstrained but less than 600 bars. The main stage fluids are compositionally similar to the parental B35 fluids, but slightly more dilute in salinity and CO_2 concentration. They were

probably derived from a cooling and depressurization path where B35 fluids cooled to B60 fluids without unmixing, and then this fluid further cooled and decompressed and mixed to some degree with meteoric waters to form main stage veins. Critical to the latter argument for main stage fluid origin is that Rusk et al. (2004) show that B60 inclusions trapped in some GS veins are Cu rich and also contain an order of magnitude more Pb, Zn, and Mn than B35 fluids. All of these metals are enriched in main stage veins.

Calculations of Hydrothermal Alteration

The equilibrium distribution of alteration mineral assemblages and hydrothermal fluid composition was computed by titrating the Butte granite into a magmatic fluid (Table 2) of composition with metal ratios based in part on bulk compositions obtained from laser ablation-inductively coupled plasma-mass spectrometry (LA-ICP-MS) analyses of Butte B35 fluid inclusions (Rusk et al., 2004). The fluid composition was further constrained by equilibrium at 600°C, 1 kbar with the following Butte alteration minerals that occur in the high-temperature potassic alteration assemblage of biotite breccias and EDM veins (e.g., Fig. 6): quartz, biotite, K-feldspar, plagioclase, andalusite, apatite, barite, magnetite, and chalcopyrite. The fluid was slightly undersaturated with muscovite.

The concentrations and concentration ratios of some critical aqueous components such as Fe, Cu, and K are set by the constraints imposed by equilibration with the mineral assemblage listed above. We independently set major cations and anions based on the LA-ICP-MS data, then constrained concentrations of other components by equilibration with the potassic alteration assemblage. Thus, the validity of a significant fraction of the initial fluid composition depends on the quality of the thermodynamic data for minerals and aqueous species. The extent by which the starting fluid composition does not fit fluid inclusion measurements or prejudices based on other constraints is a measure of questionable thermodynamic data and a measure of our inadequate understanding of the quality or meaning of independent measurements of fluid composition. One slim possibility is that the thermodynamically constrained estimate of composition is better than measurements of fluid inclusion composition. In any case, for a study such as this that is founded on thermodynamic equilibrium, we cannot depart from the equilibrium constraints.

TABLE 2. Magmatic Fluid and Rock Compositions

Species	Moles	Rock	wt %
H^+	0.58315E+01	SiO_2	65.38
H_2O	0.51900E+02	Al_2O_3	15.30
Cl^-	0.67063	Fe_2O_3	2.11
SO_4^{2-}	0.73150	FeO	2.71
HCO_3^-	0.26561E+01	MnO	0.09
HS^-	0.17108E+01	MgO	2.12
SiO_2	0.43861E-01	CaO	3.81
Al^{3+}	0.13090E-03	Na_2O	3.09
Ca^{2+}	0.11493E-03	K_2O	4.00
Mg^{2+}	0.74562E-05	P_2O_5	0.17
Fe^{2+}	0.84923E-05	BaO	0.97
K^+	0.71378E-01	CuO	0.0037
Na^+	0.34556	PbO	0.0024
Mn^{2+}	0.69967E-03	ZnO	0.0074
Zn^{2+}	0.71840E-03		
Cu^+	0.24832		
Pb^{2+}	0.15532E-03	fluid pH (590°C): 5.9	
Ag^+	0.87008E-05		
Ba^{2+}	0.26301E-05		
HPO_4^{2-}	0.72956E-06		

Calculations were executed with CHILLER (Reed, 1998; program now expanded and renamed CHIM-xpt) by eight isothermal titrations at 1-kb pressure and temperatures ranging from 200° to 600°C in 50° intervals, plus a run at 590°C. The isothermal series was augmented by four calculations at constant composition and varying temperature to define phase relations where phase boundaries were inadequately constrained by the 50°C spacing. An additional 34 computer runs enabled us to refine phase boundary details in some areas. A total of more than 5,000 composition-T-P points were computed for this study. The maximum temperature used for computing potassic assemblages by reaction of the B35 fluid with Butte granite is 600°C, which is an approximation of the true circumstance, which would have it at about 650°C (Roberts, 1973; Brimhall, 1977; Mercer and Reed, 2013). The 600°C temperature is necessitated by limitation to 600°C of thermodynamic data for aqueous species.

The thermodynamic data used in the numerical experiments described below are compiled in database SOLTHERM (Reed and Palandri, 2010a), which contains current equilibrium constants for minerals, gases, and aqueous species. All data sources are referenced in the database. Most of the equilibrium constants in SOLTHERM are computed using SUPCRT92 (Johnson et al., 1992), modified to use internally consistent mineral thermodynamic data for silicates, oxides, hydroxides, carbonates, and gases from Holland and Powell (1998; available online at http://www.esc.cam.ac.uk/research/research-groups/holland/thermocalc), but also including sulfide mineral data from a revised SUPCRT92 database, SLOP.98 (Shock et al., 1997, revised in 1998). Thermodynamic data for water and aqueous species are documented by Shock and Helgeson (1988) and Shock et al. (1997).

The calculations yield the complete mineral assemblage, compositions of solid solutions, such as chlorite, biotite, and epidote, and composition of the aqueous phase, as displayed for the 500°C titration in Figure 7. For plagioclase, we approximated the peristerite gap by defining discrete solid solutions, An20, An25, and An30. Calculation results are summarized in Figures 8 and 9 for mineral assemblages and pH over the temperature range from 200° to 600°C and a water/rock ratio of 0.01 to 100. Even though the calculations were executed by titrating granite into fluid because it is numerically expedient, the same result would follow from titrating fluid into granite. Either way, the system equations are solved for a series of discreet compositions fixed by the ratio of fluid to rock, and the computed assemblages are independent of the path taken to arrive at each computed composition.

Geochemical Modeling: Discussion

The principal finding from calculations is that one single magmatic fluid composition is capable of yielding all observed assemblages of minerals in altered wall rock and veins. To examine how this conclusion follows, we first review results from the 500°C reaction, then generalize to the whole range of temperature and composition.

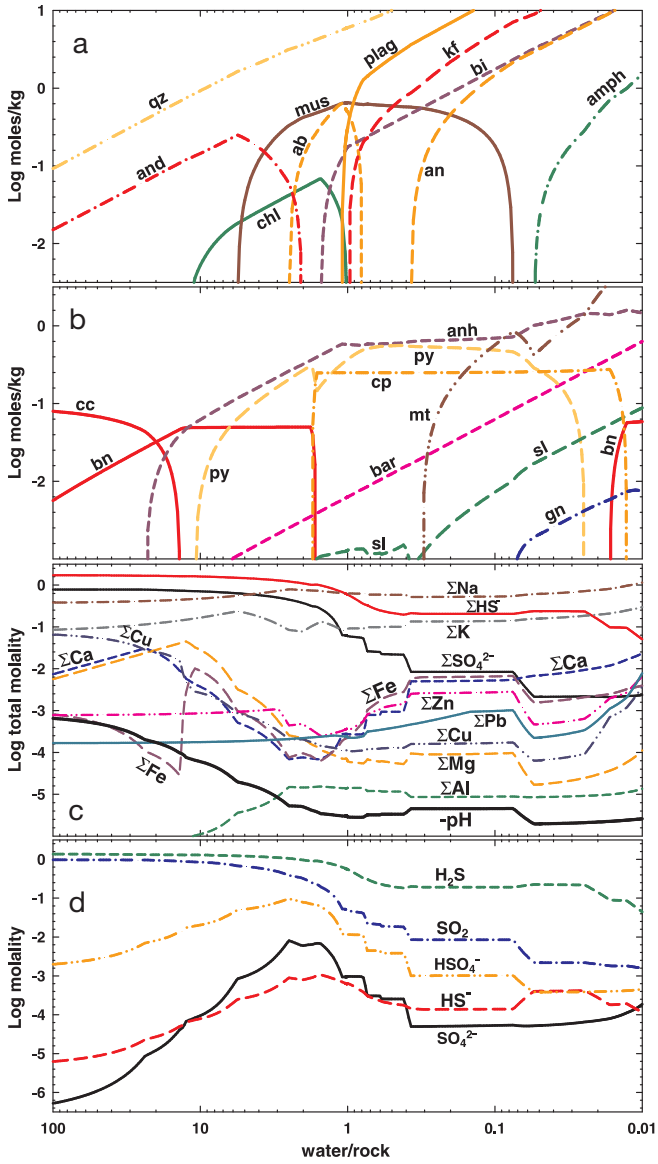

FIG. 7. Computed reaction of Butte granite with magmatic fluid at 500°C and 1 kb, showing details for a single run of the kind used to build the summary diagrams shown in Figures 8 and 9. Reactant compositions are given in Table 2. Mineral abbreviations are given in the caption to Figure 8. a) Silicate alteration minerals; "bi" refers to annite-phlogopite solid solution in which the phlogopite end member dominates at high water/rock, but the two are similar at low water/rock; "amph" refers to tremolite-ferroactinolite solid solution; "plag" refers to plagioclase solid solutions in the range of An(20) to An(30); "chl" refers to an Fe-Mg chlorite solid solution, strongly dominated by the Mg end member at high water/rock but more nearly equal between Fe and Mg end members at low water/rock. b) Ore minerals and nonsilicate alteration minerals. c) Total concentrations of the aqueous phase components. d) Concentrations of individual aqueous species relevant to understanding pH. Additional abbreviations: an = anorthite, anh = anhydrite, bar = barite, bn = bornite, cc = chalcocite, cp = chalcopyrite, gn = galena, mt = magnetite, py = pyrite, qz = quartz, sl = sphalerite.

500°C magmatic fluid reaction with Butte granite

To begin the 500°C reaction, we first cooled the starting fluid from 600° to 500°C, then titrated it with Butte granite without fractionation of minerals. At high water/rock ratio, the reaction yields andalusite and chalcocite (Fig. 7b). With further added granite (decreasing water/rock), quartz, anhydrite, chlorite, and muscovite form, as observed in a sericitic alteration assemblage (GS and PGSs, Table 1), accompanied by bornite and pyrite. Upon further reaction, the sericitic assemblage is replaced by a potassic assemblage, containing muscovite, K-feldspar, plagioclase, and chlorite, initially lacking biotite, as in the PGS alteration, then at lower water/rock, biotite replaces chlorite, as in the EDM assemblages of Butte. Computed potassic assemblages also include anhydrite, pyrite, chalcopyrite, and magnetite. The change of the thermodynamically stable mineral assemblage from sericitic to potassic is a response to the increasing neutralization of acid in the starting fluid.

The aqueous phase changes composition dramatically with change in water/rock ratio (Fig. 7c), led by a pH increase from 3.1 in the starting fluid (500°C) to a neutral value of ~5.5 at water/rock <1, where feldspars and biotite dominate the alteration assemblage. The pH is initially acidic owing to SO_2 disproportionation when the initially 600°C fluid cools to 500°C (see below). That acidity is neutralized by reaction with the granite feldspars and mafic minerals, producing andalusite and quartz, then subsequent muscovite and chlorite. Muscovite is joined by feldspars when pH reaches about 5.5, where it is buffered in concert with aqueous Na and K species, for example, by the following equilibrium:

$$2\ NaAlSi_3O_{8\,(ab)} + 2\ H^+_{\,(aq)} + KAlSi_3O_{8\,(kf)} = KAl_3Si_3O_{10}(OH)_{2\,(mus)} + 6\ SiO_{2\,(qz)} + 2\ Na^+_{\,(aq)}. \quad (1)$$

Initial sulfate and sulfide are mostly consumed by forming anhydrite, pyrite, and chalcopyrite. Aqueous Ca is transferred from fluid to anhydrite until pH becomes high enough to allow plagioclase, which then consumes aqueous Ca. Aqueous Mg is consumed by chlorite and biotite. Cu, Zn, and Pb precipitate in bornite, chalcopyrite, sphalerite, and galena. Fe changes little overall, initially entering sulfides at high water/rock ratio, then biotite and magnetite at low water/rock.

Metasomatic petrology of Butte alteration: Water/rock vs. temperature diagram

Our examination of hydrothermal alteration mineral geochemistry is based on a computational mapping into pressure-temperature-composition space (P-T-X space) of the stability fields of all minerals in our system, the compositions of solid solutions, and the composition of the aqueous phase. The composition variable refers to the 20 components we considered that are distributed among minerals and the hydrothermal fluid. To make the mineral assemblage results comprehensible in a single diagram, we display in T-X space the presence or absence of many of the minerals in the system, as shown in Figure 8. The X coordinate is water/rock, which expresses the extent of mixture along a pseudobinary coordinate between the fluid and rock compositions (Table 2).

The T vs. water/rock diagram (Fig. 8) was constructed by marking the appearance and disappearance points of each mineral along each of the nine isotherms and four iso-water/rock lines we computed, then connecting the dots. In some T-X zones, we did not have sufficient resolution from the original 13 runs to pin down phase boundaries, so we ran an additional 34 short calculations at the required temperatures

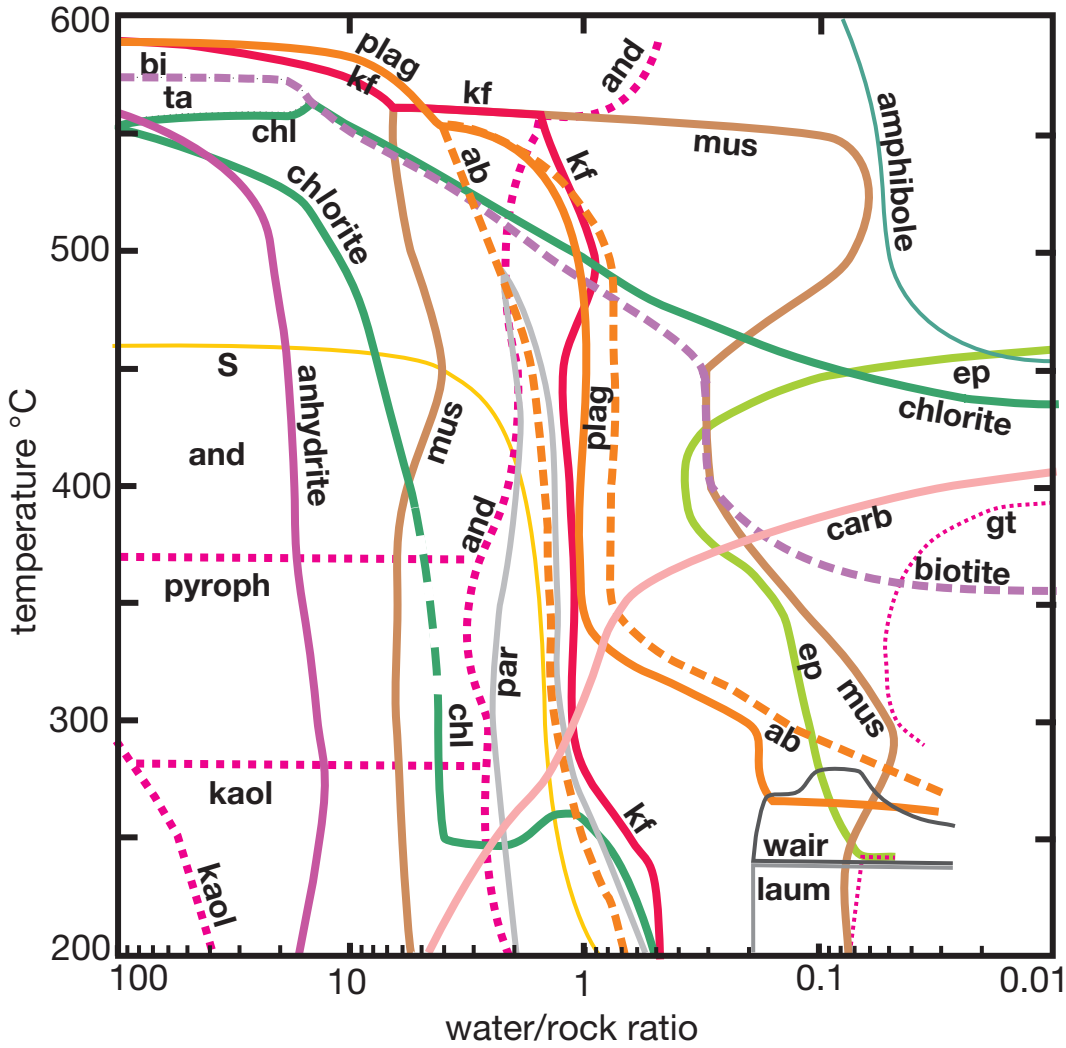

FIG. 8. Alteration mineral phase diagram showing the conditions of temperature and reaction ratio of magmatic fluid to Butte granite that controls the presence or absence of minerals. Each curve on the diagram is labeled on the side of the curve where the relevant mineral exists; the mineral is absent on the opposite side of the curve. Quartz is present throughout the T-water/rock space shown. See text for discussion of the construction and interpretation of the diagram. Some curves end near the lower right corner where the aqueous phase is entirely consumed by formation of hydrous minerals. Mineral abbreviations: ab = albite, and = andalusite, bi = biotite, carb = magnesite, rhodochrosite, dolomite, and calcite (most abundant), chl = chlorite solid solution, ep = epidote-clinozoisite solid solution, gt = garnet (andradite-grossularite solid solution), kaol = kaolinite, kf = K-feldspar, laum = laumontite, mus = muscovite, par = paragonite, plag = plagioclase, An(20) to An(30), pyroph = pyrophyllite, ta = talc, wair = wairakite.

and water/rock ratios to determine the locations of the phase boundaries. Most such points occur where we show sharp corners in phase fields, for example, where K-feldspar, muscovite, and andalusite come together. The water/rock-T diagram differs from conventional phase diagrams because each line marks the edge of a mineral stability field, not a transition from one mineral to another, although many overlapping lines do show a transition between phases.

For each mineral, we could show mineral mass by contouring in the third dimension, which would be useful for understanding alteration and ore mineral distribution, for example. Similarly, for each aqueous component or species, we could contour concentration, as we do for H^+ in Figure 9. Similar graphs of K, Ca, Cu, and Fe would be useful for understanding the transfer of metals between minerals and the hydrothermal fluid to aid in understanding alteration compositional trends and ore grade, although we do not include these figures here because our focus is on understanding alteration mineral assemblages.

Chemical equilibria and mineral assemblages in the whole fluid-rock system

The basic pattern outlined above for the 500°C example (Fig. 7) applies at temperatures lower than about 550°C, but at higher temperature, feldspars, biotite, and andalusite of the "potassic" alteration assemblage dominate even at high water/rock, as shown in Figure 8 (upper left). The potassic assemblage extends to temperatures less than 550°C, too, but only

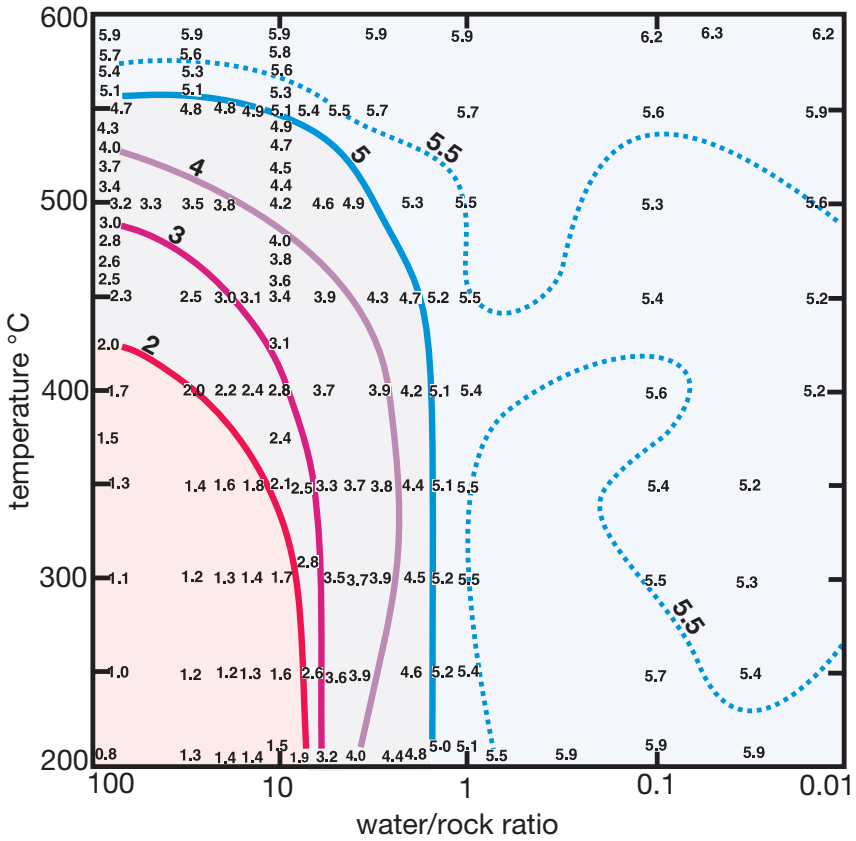

FIG. 9. Computed pH as a function of temperature and water/rock ratio, for the same calculation results depicted for minerals in Figure 8. The colored lines are iso-pH curves plotted with respect to the numerical pH values, some of which are shown. The pH values are highly acidic at lower temperatures and high water/rock ratios (red shading) and neutral at all high temperatures and at low water/rock ratios (blue shading). This pattern reflects the acid production by SO_2(aq) disproportionation with decreasing temperature (reaction 2) and acid neutralization by reaction with granite.

at water/rock larger than 1. At lower temperatures, where epidote and chlorite are present along with feldspars, the potassic alteration grades into propylitic. At water/rock between 1 and 5, chlorite, muscovite, and quartz are dominant, as in "sericitic" alteration, and at larger still water/rock, aluminum silicates and quartz dominate, as in advanced argillic alteration.

The cause of the particular mineral distribution pattern described above is that the magmatic fluid is pH neutral at high temperature but acidic at temperatures less than 550°C, as shown in Figure 9. For example, the same fluid that is in equilibrium with feldspars and biotite at 600°C and pH 5.9 is so acidic at 500°C, pH 3, that it forms quartz and aluminum silicates. The reason for the neutral-to-acidic pH change with decreasing temperature is that SO_2(aq), or its equivalent, H_2SO_3(aq), is the dominant sulfur species at high temperature, but it disproportionates with decreasing temperature, forming sulfuric acid and H_2S, as in the following reaction:

$$SO_{2\,(aq)} + H_2O_{\,(aq)} = 1\tfrac{1}{2}\,H^+_{\,(aq)} + \tfrac{3}{4}\,SO_4^{2-}{}_{(aq)} + \tfrac{1}{4}\,H_2S_{\,(aq)}. \quad (2)$$

Between 600° and 100°C, the equilibrium constant for reaction (2) increases by 17 orders of magnitude (10^{-15}–10^{2}), shifting the reaction strongly to the right at lower temperature, yielding hydrogen ions. This effect is illustrated in Figure 10, which shows H^+ activity and molalities of the dominant sulfur species and HCl in the Butte granite reaction at water/rock = 10; molalities shown in Figure 10 are affected not only by reaction (2), but also by equilibria involving aluminum silicates, quartz, native sulfur, sulfides, and sulfates, as shown in Figures 7 and 8 at water/rock = 10.

The role of sulfur species in controlling pH is strongly dominant over that of HCl, which plays a minor role in supply of H^+ to the hydrothermal fluid (Fig. 10). The most significant role of Cl^- is in transport of metals in chloride complexes. The minor role of HCl relative to sulfur acids is dictated by the aqueous mineral equilibria that partition far more Cl^- to NaCl and KCl than to HCl at high temperature, where pH is controlled by feldspar-mica equilibria, as shown in Figure 10.

"Wrong" assemblages

Some assemblages apparent in the water/rock vs. T diagram (Fig. 8) do not correspond to known natural counterparts in Butte or elsewhere. Two examples are (1) the appearance of K-feldspar largely overlapping with plagioclase at temperature exceeding 350°C, leaving inadequate space in water/rock for the common assemblages containing K-feldspar, but lacking plagioclase, and (2) the large field of native sulfur extending to low water/rock and thereby overlapping excessively with muscovite. These questionable phase boundaries, and others,

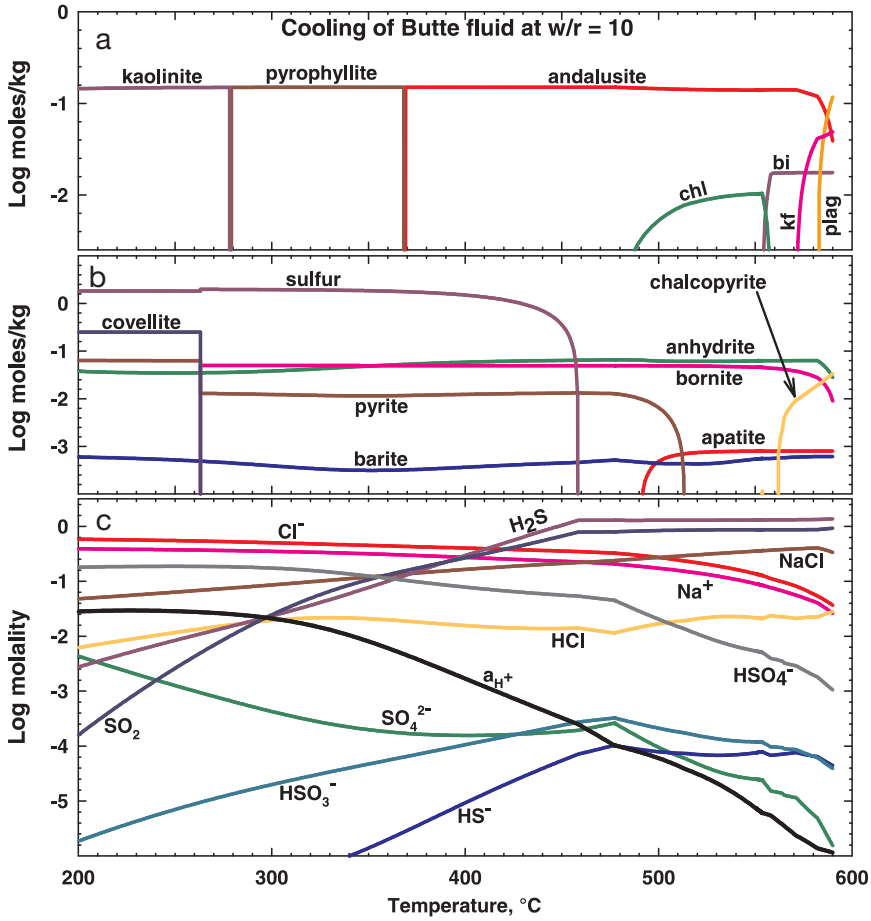

FIG. 10. Computed cooling of reacted fluid from 600° to 200°C for the water/rock = 10 reaction. The minerals and fluid composition shown here match those for a vertical line at water/rock = 10 in Figures 8 and 9. a) Silicate alteration minerals, b) nonsilicate alteration minerals, and c) concentration of aqueous species relevant to understanding pH. Particularly notice that pH changes from 6 at 600°C to 1.6 at 200°, as SO_2(aq) disproportionates upon cooling. See text and reaction 2.

result from (1) deficiencies in thermodynamic data for minerals or aqueous species, (2) inapplicability of the simple water-rock reaction model and the particular pressure of this study (1 kb), (3) starting with the "wrong" magmatic fluid composition, or (4) incomplete and insufficiently careful petrography on the natural assemblages. Mismatches between what we compute and what we see stimulate new observations, new experimental measurements, and insights into how the natural system works.

Concerning the "wrong" starting magmatic fluid, we have executed several calculation sets varying concentrations of SO_2, H_2S, and SO_4^{2-}. The effects can be surprising. For example, increased sulfate yields increased anhydrite, which results in less plagioclase precipitation, thereby yielding excess aqueous aluminum, which enlarges the field of andalusite in the potassic assemblages. The nonlinear feedback apparent in this example (increased sulfate enlarges andalusite) illustrates the complexity of such multicomponent systems, and suggests how subtle effects make "wrong" assemblages. Among the variations we explored, we obtained some assemblages more nearly resembling those at El Salvador, Chile (Gustafson and Hunt, 1975), than those at Butte by using a more acidic and sulfur rich fluid than applied here (Table 1).

There are many more such effects to be explored. For example, at pressures lower than 1 kb, the stability field of K-feldspar is enlarged at the expense of muscovite, thereby enlarging the temperature-composition range of potassic alteration relative to that of sericitic. We know that pressure changed from lithostatic to hydrostatic as the Butte system evolved (Rusk et al., 2008a). The pressure drop caused quartz to precipitate in veins, K-feldspar to replace sericite in potassic alteration envelopes (Reed, 1997), and the fluid to separate into a brine and vapor. These processes complicate the picture considerably. The conclusion is that the view presented here is but one slice through the exceedingly complex P-T-composition-time history of the natural system.

Fluid-rock chemical contact and centimeter-scale alteration zoning

The chemical effects outlined above can be tied to the Butte veins and their zoned envelopes (Figs. 4, 5) by considering the physical setting, wherein a magmatic fluid advects on a scale of kilometers through a fracture system while exchanging chemical species with wall rock through diffusion on a scale of centimeters. Where magmatic fluids are in contact with fresh wall rock along newly opened hydrofractures, chemical

species in the fluid such as H^+, K^+, and H_2S diffuse down concentration gradients distances of millimeters to centimeters through water-wet cleavage openings in plagioclase and biotite and along water-wet mineral grain boundaries. Along the diffusion pathway, the aqueous species react with primary wall-rock minerals or with already-formed alteration minerals, ultimately yielding zoned alteration envelopes. Aqueous reaction products from breakdown of primary minerals, e.g., Na^+ and Ca^{2+} from feldspars, diffuse in the opposite direction along the same water-wet pathways from the altered wall rock to the fracture where they are advected away with the throughgoing hydrothermal fluid.

The time scale of such diffusion and reaction is probably on the order of years to tens of years, as estimated for Butte GS alteration at 400°C by Geiger et al. (2002), which is much longer than the time scale of initial hydrofracturing and fluid injection in single fractures. The bulk fluid and the bulk rock never reach overall chemical equilibrium, but the fluid and alteration minerals do equilibrate at a scale of millimeters to centimeters, as can be appreciated by recognizing that observed mineral assemblages match computed thermodynamically stable assemblages at the scale of diffusion envelopes, as explained below.

As diffusion and reaction proceed, zoned alteration envelopes form like the examples described above, such as PGSs/PGSk/EDM alteration (Table 1), which encompasses a transition from an innermost sericite-quartz assemblage lacking K-feldspar, to one with K-feldspar but no biotite, to an outmost assemblage containing K-feldspar and biotite. A similar transition occurs in GS/DGS zoned envelopes, from an assemblage lacking K-feldspar (GS) to one containing K-feldspar (DGS). Wall rock that is near the fracture has ready access to the bulk fluid through short diffusion distances and develops "fluid-dominated" mineral assemblages characteristic of high water/rock ratio, such as those of advanced argillic and sericitic alteration that plot at high water/rock in Figure 8. Distal wall rock in the envelope has less fluid access and develops "rock-dominated" assemblages characteristic of low water/rock that plot at low water/rock in Figure 8 (right side). The lesser fluid access for distal rock is valid, but the effect is really that the concentrations of species arriving at a distal point have been diminished by reaction along the way; thus, the distal fluid has already evolved in the direction of lower water/rock.

A single zoned envelope can be represented by a short horizontal (isothermal) line in Figure 8, spanning the innermost to outermost assemblages from high water/rock to low water/rock. For example, the progression from assemblages characterized by muscovite-chlorite to muscovite-chlorite-K-feldspar, to muscovite-K-feldspar-biotite, matches the progression observed from the vein outward in PGS/EDM alteration envelopes, as shown in Figure 4e and represented by a horizontal line at "P" in Figure 11. Such envelopes reflect high-temperature progressive neutralization of an initially acidic fluid.

District-scale alteration zoning

Along the kilometer-scale fluid infiltration pathway where the bulk fluid advects outward through the open fracture system, proximal (deep) wall rocks are in contact with relatively unreacted hot fluid and develop a fluid-dominated assemblage of high water/rock (left side of Figs. 8, 11). Distal rock is visited by advected fluid that has already reacted with rock along the way and is thus closer to equilibrating with the wall-rock minerals. Consequently, rock-dominated assemblages of low water/rock form in distal settings (right side of Figs. 8, 11).

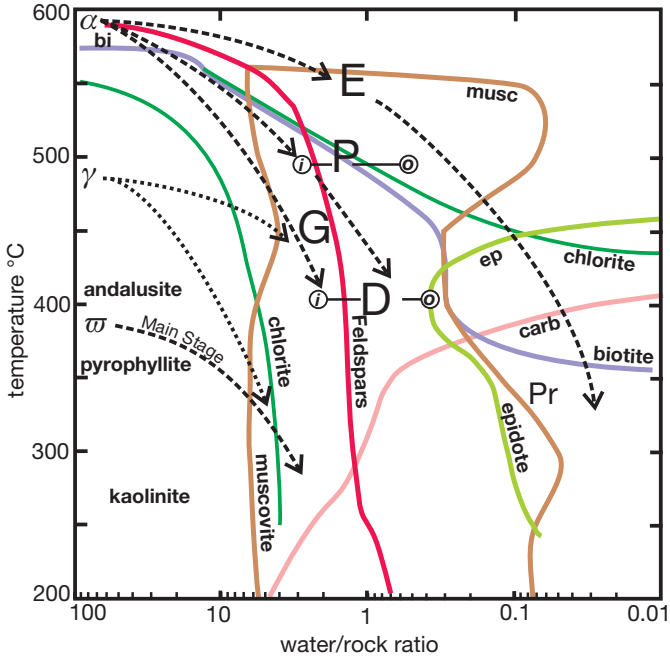

FIG. 11. Mineral stability relative to temperature and water/rock reaction ratio, as in Figure 8, but simplified to show fluid reaction trajectories and alteration mineral assemblages observed in Butte and other porphyry copper deposits. Letters E, P, G, D, and Pr refer to EDM, PGS, GS, DGS, and propylitic alteration, respectively, as described in Table 1 and in the text. The circled "i" and "o" tied by horizontal lines to "P" and "D" refer to the mineral assemblages of the inner (i) and outer (o) zones of alteration envelopes that are otherwise designated as PGS and DGS. Notice that the inner envelopes connected to PGS and DGS alteration are the same assemblage as in GS, consisting of quartz, chlorite, and muscovite, but lacking feldspars. "α" refers to magmatic fluid as observed in B35 inclusions, which reacts and cools along trajectories shown by dashed curves to generate the potassic vein series described in the text. "γ" refers to fluid observed in B60 inclusions interpreted as a cooled and depressurized α fluid responsible for generating the GS veins that are abundant in the center of the district (Figs. 1, 3). "ω" refers to a further cooled and depressurized fluid responsible for main stage vein mineralization.

Early veins: The biotite-K-feldspar series: The deep-to-shallow progress through the vein series described above, EDM, PGS, GS, DGS, and propylitic, can be understood with reference to the ascent, cooling, and reaction of a deep fluid with Butte granite. A 600°C fluid produces a potassic assemblage at depth (point α, Fig. 11) such as that of EDM veins (Fig. 4d) and biotite breccias (Fig. 4a). As that fluid followed an outward path of moderate cooling (α to E, Fig. 11), it would produce EDM alteration at temperatures greater than 450°C, then distal propylitic assemblages at temperatures below ~400°C and low water/rock ratios, such as in the chlorite-epidote assemblage at Pr in Figure 11, accompanied by feldspars and carbonates with sphalerite, galena, and rhodochrosite in small veinlets, as observed in distal propylitic alteration at Butte.

If the same 600°C fluid followed a path resulting in more rapid cooling relative to wall-rock reaction (α to P, Fig. 11), it would become somewhat acidic, producing quartz, biotite, and feldspar early, then, further down on its trajectory, yielding sericite-chlorite alteration (P-*i* at left of *i*-P-*o* line, Fig. 11), which would form an inner envelope of sericite-chlorite with no K-feldspar (PGSs, Table 1) that is bordered outward by PGS alteration with feldspar (PGSk), then biotite assemblages (P-*o*, right end of *i*-P-*o* line). This particular sequence is observed in Butte PGS/EDM alteration envelopes (Fig. 4e). Further traverse of the alpha fluid beyond P to D in Figure 11 yields shallow DGS assemblages characterized by feldspars, sericite, and chlorite replacing biotite. Finally, after further cooling and reaction with slightly more rock, that fluid yields epidote-bearing propylitic assemblages (Pr).

In the periphery of the Anaconda and Pittsmont domes the alteration envelopes on some pyritic veins of gray sericite-chlorite-pyrite-quartz (GS) with an outer DGS halo (GS/DGS) likely formed by a fluid trajectory with limited rock reaction (α to D-*i,* the left end *i*-D-*o* line, Fig. 11). This fluid trajectory entails substantial cooling without much acid neutralization, producing an acidic fluid that forms the GS veins, with or without a distinct outer DGS envelope. Such veins are pyritic with little chalcopyrite (e.g., Fig. 4b) and closely resemble the GS veins formed later in the center of the district (Figs. 1, 3) by fluids of the same chemical character.

The fluid trajectories described above for the Butte parent fluid originating at alpha in Figure 11 are a sampling of an infinite number of paths that upwelling fluids may take through the fracture system, including variations not addressed here, such as phase separation yielding derivative fluids identified in halite-bearing fluid inclusions (B15h) and vapor-rich fluid inclusions (B85; Rusk et al., 2008a). The large number of different histories for individual fluid parcels yield the large number of alteration patterns observed in the Butte alteration envelopes. For example, EDM veins lack an inner PGS zone, as at E in Figure 11. However, an alpha fluid that cools more becomes slightly acidic and yields a PGS/EDM envelope that lacks biotite in the innermost zone, as depicted at P-*i* in Figure 11. Such PGS/EDM envelopes formed from a fluid trajectory from alpha to a point in the feldspar field (near P, Fig. 11). Similarly, there are many envelopes of DGS only, lacking an inner envelope of GS alteration, and others that are propylitic only, lacking an inner DGS envelope. In all such cases, the fluid trajectory involves enough rock reaction along the way to neutralize some of the acidity so the fluid is capable of producing the alteration characteristic of lower water/rock as at points D and Pr in Figure 11.

Quartz-sericite-pyrite veins: GS alteration: Over time the cupola fluid reservoir cools, making an acidic fluid such as that identified at gamma in Figure 11, which resembles the moderate-density fluid in B60 fluid inclusions at Butte. Based on the results of Rusk et al. (2008a), we infer that the B60 fluid was derived from the B35 fluid (magmatic fluid; α, Fig. 11) by modest cooling from 650°C and depressurization without phase separation. Emergence of a 480°C fluid along a reaction-cooling path (γ to G, Fig. 11) makes the central mushroom-shaped GS alteration zone (Fig. 3), the veins of which cut all early vein types, yielding the characteristic pyrite vein fillings with a halo of sericite, quartz, pyrite, and colorless chlorite (Fig. 5b, c). The colorless chlorite lacks iron, which is the same as is computed (e.g., x(Mg-chl) = .9998) for the high water/rock chlorites (Fig. 8, left part of chlorite field), owing to removal of iron into pyrite. The B60 (gamma) fluids are distinctive for containing elevated Cu concentrations (Rusk et al., 2004) even though they formed a large volume of Cu-poor rock (<0.15% Cu), an effect resulting from the fluid's intense acidity, which diminished Cu precipitation, particularly at the high temperatures of GS alteration (>400°C).

The GS/SBr veins that are common in the central GS zone (Fig. 5c, d) reside in the T-water/rock region designated as GS (G, Fig. 11). As explained above, the same GS assemblage can be formed by cooling and reaction of the alpha fluid (Fig. 11), which is what produces the GS veins in the periphery of the Anaconda and Pittsmont domes. The SBr alteration lacks newly formed biotite, as in EDM alteration, but includes residual granite biotite, partially converted to muscovite, and surrounded by sericite-replaced feldspars. Thus, the SBr reflects incomplete GS formation, but apparently under sufficiently sulfidic conditions that green chlorite does not form (as it does in GS/DGS alteration).

By analogy in timing and mineral assemblage, the late sericite-quartz-pyrite alteration that is common in porphyry copper deposits worldwide probably forms from the late escape of a cooled magmatic fluid such as the gamma fluid of Figure 11, as opposed to a fluid newly evolved from magma, which cannot be acidic enough to produce sericitic alteration until it cools below 550°C. Further cooling of such a fluid yields a late mineralizing fluid capable of producing the Butte main stage.

Main stage veins: Cooling of the parent fluid to less than 380°C (Rusk et al., 2008b) yields an acidic fluid shown at omega in Figure 11, with a pH less than 2 (Fig. 9). The fluid produces intense advanced argillic alteration upon reaction with the Butte granite, making quartz, topaz, pyrophyllite, and kaolinite in inner alteration envelopes, and sericitic assemblages outward from the advanced argillic zone, as documented by Meyer et al. (1968). At temperatures less than ~400°C, the andalusite (Al_2SiO_5) of Figure 8 is a proxy for the topaz ($Al_2SiO_4(OH)_2$) commonly observed in advanced argillic alteration at Butte and elsewhere. Advanced argillic alteration is abundant in the Butte horsetail veins of the Leonard mine and along main stage veins that traverse eastward and westward beyond the zone of intense GS alteration in the center of the district (Fig. 1). The deepest known occurrences of such advanced argillic alteration, including topaz, are in envelopes of quartz veins, some with enargite, deep in the center of the district (~250 m below sea level in the bottom of drill hole 1A, Fig. 3).

The acidic omega fluid precipitates sulfides of the "high-sulfur assemblage" (Meyer and Hemley, 1967) including covellite, enargite, digenite, and pyrite (e.g., Fig. 5b), which, along with advanced argillic alteration, are characteristic of the Butte main stage horsetail ores and analogous late veins in many other porphyry copper systems, for example, Superior, Arizona (Manske and Paul, 2002), Chuquicamata (Ossandón et al., 2001), El Salvador (Gustafson and Hunt, 1975), and Collahuasi, Chile (Masterman et al., 2005), which are deep geochemical equivalents of the somewhat cooler

high sulfidation ores, such as at Pascua, Chile (Chouinard et al., 2005), Summitville, Colorado (Stoffregen, 1987), the Nansatsu ores of Kyushu, Japan (Hedenquist et al., 1998), and Lepanto-Far Southeast, Philippines (Hedenquist et al., 1998).

Meyer and Hemley (1967) laid out the direct role of strongly acidic conditions in a sulfidic fluid in producing the high-sulfur mineral assemblage linked to advanced argillic alteration. It is now apparent that sulfuric acid and H_2S are produced from a magmatic source by way of SO_2 disproportionation (reaction 2), and that they drive reactions such as the following, which show how covellite (cv) and enargite (en) are stabilized by acid and H_2S relative to lower-sulfur alternatives, chalcocite (cc) and tennantite (tn), respectively:

$$2\,CuS\,(cv) + H_2O_{(aq)} = Cu_2S\,(cc) + \tfrac{1}{4}SO_4^{2-}{}_{(aq)} + \tfrac{1}{2}\,H^+{}_{(aq)} + \tfrac{3}{4}\,H_2S_{(aq)}, \text{ and} \quad (3)$$

$$4\,Cu_3AsS_4\,(en) + 3\,H_2O_{(aq)} = Cu_{12}As_4S_{13}\,(tn) + 1\tfrac{1}{2}\,H^+{}_{(aq)} + 2\tfrac{1}{4}\,H_2S_{(aq)} + \tfrac{3}{4}\,SO_4^{2-}{}_{(aq)}. \quad (4)$$

These reactions and others in the series from high to low sulfidation, i.e., chalcocite to bornite and bornite to chalcopyrite, both with added pyrite (Reed and Palandri, 2006), are written to species that are abundant in the aqueous phase, H^+, H_2S, SO_4^{2-}, as opposed to S_2(gas), for example, thereby providing an intuitively clear link between what we know of the fluid and what we observe in the field (cf. Einaudi et al., 2003). Geochemical models of precipitation of pyrite, enargite, covellite, and native sulfur by cooling, boiling, and cold water mixing are given in Saunders et al. (2013) in relation to precipitation of "high sulfidation" epithermal ores (or acid sulfate Cu-Au ores, e.g., Nansatsu, Summitville, Pascua, Lepanto), and Einaudi et al. (2003) provide a cogent review and discussion of the geologic and geochemical settings of the high sulfidation assemblage.

As the highly acidic omega fluid identified in Figure 11 reacts with wall rock, after initially producing advanced argillic alteration, it yields sericitic assemblages, which would border veins containing bornite and chalcopyrite, then, more distally, sphalerite, galena, and Mn carbonates, as observed in the Butte main stage zoning pattern (Meyer et al., 1968). Fluids trapped in B60 fluid inclusions (see above) are likely parents of the main stage fluid (omega, Fig. 11) as argued by Rusk et al. (2008a). Although sphalerite is commonly prevalent in distal reaches of porphyry-related base metal veins, it does accompany high sulfidation Cu assemblage (covellite, digenite, enargite) in the East Colousa horsetail ores north of the Leonard mine (Meyer et al., 1968) and in similar veins at Chuquicamata (Ossandón et al., 2001). Similarly, sphalerite and galena occur with high sulfidation assemblages in some acid-sulfate Cu-Au ores, such as Iwato, Japan (Hedenquist et al., 1994). This point is significant for showing that the copper ores precipitate from a fluid that also contains significant Zn, and likely also Pb and Mn, as in the Butte B60 inclusions (Rusk et al., 2004), but sphalerite and galena mostly do not precipitate with the high-sulfur copper minerals because aqueous Pb and Zn are not sufficiently concentrated to form sulfides under the acidic conditions, and Mn carbonate certainly requires more neutral pH.

Upon cooling of a magmatic fluid, SO_2 disproportionation (reaction 2) and consequent production of acidic fluids are an inevitable end-stage in the emplacement and cooling of a porphyry copper system, which is why so many porphyry copper deposits contain advanced argillic alteration (e.g., Sillitoe, 2010) and why it is always late. A similar conclusion is implied by Einaudi et al. (2003) in their discussion of the relationship of the high sulfidation vein ores to porphyry copper deposits. In systems where the late advanced argillic system is poorly developed, its lack of development may reflect exhaustion of fluid in forming higher-temperature mineralization, leaving none for late veins, or it may reflect fluid expulsion to the surface in shallow systems. At Butte, Superior, Chuquimata, and many others, a substantial quantity of omega fluid emerges late to yield high sulfidation mineralization with advanced argillic alteration. Considering the likely simultaneity of sericitic alteration occurring at depth while advanced argillic forms above it, a late collapse of the upper acidic fluid into the sericitic zone is possible, as opposed to a late emergence of new magmatic fluid from a cupola.

At temperatures below 400°C, the omega fluid (Fig. 11) is acidic enough (Fig. 9) to dissolve out chalcopyrite previously precipitated in the potassic vein series, remobilizing it into main stage veins elsewhere, as suggested by Brimhall (1979). Leaching by main stage fluids occurs in limited volumes along pyritic main stage veins that traverse the deep northeastern Anaconda dome. The meter-scale alteration envelopes on these veins are characterized by white sericite and much lower Cu grades than the surrounding rock, although the Mo grades are unchanged. This late main stage leaching is distinct from the partial Cu leaching in pre-main stage late GS time where the stockwork of pyritic veins of the central GS zone overlap the western edge of the Pittsmont dome.

Quartz-molybdenite veins: Veins of quartz alone (barren quartz) or quartz and molybdenite grade into each other at depth, cut the early veins of the potassic series (Fig. 4a), and are mostly cut by GS veins (there are rare reversals). Although quartz-molybdenite veins are early in the temporal sequence, they differ from the EDM, PGS, and DGS veins in lacking alteration everywhere except in their deep occurrences in the Pittsmont and Anaconda domes, where many have millimeter-scale borders of K-feldspar ± biotite, and thus resemble EDM veins. The B35 fluid inclusions in the quartz-molybdenite and barren quartz veins are indistinguishable from those in deep EDM veins in every respect, including composition determined by Raman spectroscopy, freezing point depression, and LA-ICP-MS (Rusk et al., 2004, 2008a). Most notably, the quartz-molybdenite B35 inclusions contain abundant Cu and Fe.

If the quartz-molybdenite fluid is the same as those in EDM veins, the lack of alteration on quartz-molybdenite veins indicates that the fractures they occupy remained open to fluid passage for such a short time that diffusion-reaction halos did not form. The tens-of-years diffusion-reaction rates modeled by Geiger et al. (2002) suggest that the quartz-molybdenite veins probably remained open no more than a few years, if that. An alternative interpretation of the lack of alteration is that quartz-molybdenite veins are somehow the product of a transient distinct magmatic differentiation effect that yields a fluid that is chemically unreactive to granite—apparently

lacking SO_2, in this case. However, such a magma would first produce a reactive fluid yielding the potassic series, then the inert fluid yielding quartz-molybdenite veins, then reactive fluids again, yielding intense sericite-pyrite and advanced argillic alteration. Such a magmatic differentiation effect is unknown and unlikely.

We interpret the quartz-molybdenite veins as the product of a pressure quench (Rusk and Reed, 2002) as fluid passes from a lithostatic to a hydrostatic regime and precipitates quartz that plugs the fractures. Vein fillings overwhelmingly dominated by quartz with additional feldspar, sulfides, magnetite, and pyrite form in computed equilibrium adiabatic decompression (Reed and Palandri, 2010b) of the same fluid (Table 2); however, it is not clear whether equilibrium is achieved between fluid and vein minerals in forming quartz-molybdenite veins in the natural setting.

Timing of quartz-molybdenite veining: Vein cutting relations place quartz-molybdenite veins largely after the potassic vein series (EDM-PGS-DGS) and almost entirely before the quartz-sericite-pyrite veins of the central GS zone, as is also common in other porphyry copper deposits. Fluid inclusion data (Rusk et al., 2008a) and the calculations presented above show that the difference between the potassic series and the later quartz-sericite-pyrite veins is largely a difference in temperature, from greater than 600°C to less than 500°C. Given that the quartz- molybdenite veins form largely by pressure quench of the same fluid that makes the potassic series, its timing between the two other veins series is apparently not tied to a magmatic differentiation process (cf. Candela and Holland, 1986), but may result from a rock mechanical evolution of the magmatic-hydrothermal system that occurs during cooling to less than 550°C, as discussed by Fournier (1999).

Conclusions

The neutral-to-acidic pH change caused by SO_2 disproportionation (reaction 2) with decreasing temperature is the essential reason that a magmatic fluid of a single composition is capable of producing all alteration types observed in porphyry copper deposits and their distal or overlapping epithermal offspring that are equivalent to the Butte main stage. The same fluid composition can produce potassic alteration at 600°C and advanced argillic alteration at 200°C, and can form quartz-molybdenite veins without alteration. The occurrence of the classical assemblage of porphyry copper deposit alteration types—potassic, sericitic, propylitic, and advanced argillic—is plausibly entirely a consequence of their origin from a single fluid composition, the temperature and extent of wall-rock reaction of which change as the system evolves. The reason veins with sericitic alteration always cut those with potassic alteration and veins with advanced argillic alteration cut those with sericitic is that as monogenetic magmatic-hydrothermal systems cool, fluids change from neutral to acidic pH through time. For example, sericitic alteration always cuts potassic because sericitic alteration always requires lower-temperature fluids than potassic, and lower temperatures always occur after hotter temperatures. Of course, the term "always" overstates the case; reversals in cutting relations most likely reflect departure from monotonic cooling owing to new fluids from renewed magma input or renewed fracturing that allows hot fluids to ascend into cooler rock.

Differences in the volume of the various alteration and ore types from one porphyry copper deposit to another may reflect differences in the timing of storage and expulsion of fluids—all postmagmatic. If all fluid is expelled early (e.g., fluid alpha, Fig. 11), it would form the potassic vein series and be finished, and that series would include distal sericitic and distal propylitic alteration, as at the points labeled Pr and G in Figure 11. If some of the initially 650° fluid is retained in a cupola, then expelled at ~480°C (e.g., fluid gamma, Fig. 11), it produces a volume of sericitic alteration as in the central GS zone in Butte or the pervasive sericitic alteration at Superior (Manske and Paul, 2002) or Chuquicamata (Ossandón et al., 2001), for example. That second fluid expulsion would make a second set of sericitic veins that would overprint the potassic series as it does in the Butte central GS zone (Fig. 3). On the basis of detailed mapping of veins, alteration, and porphyry cutting relations, Seedorff and Einaudi (2004b) make a similar argument for the relationship between early potassic and later sericitic alteration at Henderson.

Deep drilling in Butte reveals a setting for possible temporary fluid retention in and above a cupola. The deep quartz vein stockwork intersected in drilling beneath the Pittsmont dome and in the center of the district (Fig. 3) appears to be the upper reaches of a volume of intensely fractured rock overlying a porphyry cupola that lies directly beneath the enormous body of Butte Cu and Mo mineralization. The proximity of the stockwork to a cupola is further indicated by the 500-m drill hole span of numerous meter-scale porphyry dikes and breccias plus the exceptionally large porphyry dikes in drill hole 1A (Fig. 3). Fluids expelled from the cupola in response to lithostatic to hydrostatic pressure transitions probably created the quartz stockwork. The pervasively sericitized rock in the stockwork zone attests to the expulsion of a large volume of fluid cooled to less than 500°C (fluid gamma, Fig. 11) that could plausibly have been held in the cupola and its stockwork-veined carapace.

A further release of fluid at 380°C (omega, Fig. 11) could have produced the fissure-filling base metal veins with advanced argillic alteration in the Butte main stage and in similar examples such as Superior, Chuquicamata, Collahausi, and El Salvador. However, some of the sericitic alteration deep in the central GS zone (Fig. 3) yields Ar-Ar dates ~1 to 2 m.y. younger than the potassic series veins (Snee et al., 1999), and Dilles (pers. comm., 2012) has pointed out that a 1- to 2-m.y. span between the Butte potassic vein series and the main stage may be too long plausibly to maintain a fluid temperature of 380°C. Thus, in the Butte case, a renewed magmatic fluid input may be necessary—apparently fluid transported from great depth and cooled in transit without sufficient wall-rock reaction to neutralize its acidity. The fluid had to have been acidic enough to produce intense advanced argillic alteration in the Butte Horsetail zone (Meyer et al., 1968) and the topaz adjacent to enargite-pyrite veins shown in Figure 3.

The Butte main stage base metal veins and similar late veins in other porphyry copper systems are deeper and hotter variants of epithermal veins that form from the same omega fluid at shallow depth (Sillitoe, 2010). It is chemically feasible to form the full range of magma-centered epithermal deposits from high to low sulfidation, where the omega fluid cools,

boils, mixes with cold meteoric waters, reacts with wall rock, is diluted while buffered by wall-rock reaction, and mixes with descending acidic fluids—all processes examined elsewhere (Spycher and Reed, 1989; Reed, 1997; Reed and Palandri, 2006; Saunders et al., 2013).

The geochemical modeling presented here has inadequacies stemming from uncertain thermodynamic data, approximations of chemical properties, and an oversimplification of the complex flow-reaction system. The inadequacies show up in the form of "wrong assemblages" and over- and underestimated concentrations of critical aqueous species, notably transition metals. Nevertheless, the relationships among minerals in alteration assemblages are largely valid, and the role of aqueous SO_2 in controlling pH as a function of temperature provides a powerful independent explanation for observations of the spatial and thermal arrangement of hydrothermal alteration assemblages.

If, as the modeling suggests, one fluid composition actually does function in the natural setting, then beyond discerning how magma chemistry controls the composition of that fluid, our analysis of the causes of the wide variation in mineral assemblages, vein types, and ore mineral assemblages must focus on understanding the geochemistry in the hydrothermal system, not the geochemistry of a hypothetical variation in hydrothermal fluid composition as a function of magma crystallization. Of course, magma chemistry is central to understanding the mix of metals, ligands, and acids that make an initial hydrothermal fluid, leading to differences among deposits dominated by Cu, Sn, W, and Mo, for example. And, certainly, many single systems produce multiple magma batches, each of which yields a similar aqueous fluid, e.g., Yerington (Profett, 1979; Carten, 1987) and Henderson (Seedorff and Einaudi, 2004a, b). The key point is that most within-deposit varieties of veins and alteration result from the response of one fluid composition to the effects of temperature and wall-rock reaction within the hydrothermal system.

Acknowledgments

This research was funded in part by National Science Foundation grants EAR 0440198 and EAR 0507181. We acknowledge the use of the University of Oregon's CAMCOR analytical facilities, which were established with a combination of federal and state funds. We thank Steve Czehura and Dick Berg for assistance in access to the Butte mine and samples. Discussions with Celeste Mercer, John Dilles, and Robert Fournier were valuable in refining some of the ideas expressed here. Discussions in the more distant past with Charles Meyer were important in shaping ideas and the approach to understanding the complexities of porphyry copper systems. We also thank reviewers Noel White and David Cooke, who provided valuable criticism that substantially improved the manuscript.

REFERENCES

Brimhall, Jr., G.H., 1977, Early fracture-controlled disseminated mineralization at Butte, Montana: Economic Geology, v. 72, p. 37–59.

——1979, Lithologic determination of mass transfer mechanisms of multiple-stage porphyry copper mineralization at Butte, Montana: Vein formation by hypogene leaching and enrichment of potassium-silicate protore: Economic Geology, v. 74, p. 556–589.

Candela, P.A., and Holland, H.D., 1986, A mass transfer model for copper and molybdenum in magmatic hydrothermal systems: The origin of porphyry-type ore deposits: Economic Geology, v. 81, p. 1–19.

Carten, R.B., 1987, Sodium-calicum metasomatism: Chemical, temporal, and spatial relationships at the Yerington, Nevada, porphyry copper deposit: Economic Geology, v. 81, p. 1495–1519.

Chouinard, A., Williams-Jones, A., Leonardson, R., Hodgson, C., Silva, P., Tellez, C., Vega, J., and Rojas, F., 2005, Geology and genesis of the multistage high-sulfidation epithermal Pascua Au-Ag-Cu deposit, Chile and Argentina: Economic Geology, v. 100, p. 463–490.

Cline, J.S., and Bodnar, R.J., 1991, Can economic porphyry copper mineralization be generated by a typical calc-alkaline melt?: Journal of Geophysical Research, v. 96, p. 8113–8126.

Einaudi, M.T., Hedenquist, J.W., and Inan, E.E., 2003, Sulfidation state of fluids in active and extinct hydrothermal systems: Transitions from porphyry to epithermal environments: Society of Economic Geologists Special Publication 10, p. 285–313.

Fournier, R.O., 1999, Hydrothermal processes related to movement of fluid from plastic into brittle rock in the magmatic-epithermal environment: Economic Geology, v. 94, p. 1193–1211.

Geiger, S., Haggerty, R., Dilles, J.H., Reed, M.H., and Matthai, S.K., 2002, New insights from reactive transport modelling: The formation of the sericitic vein envelopes during early hydrothermal alteration at Butte, Montana: Geofluids, v. 2, p. 185–201.

Gustafson, L.B., and Hunt, J.P., 1975, The porphyry copper deposit at El Salvador, Chile: Economic Geology, v. 70, p. 857–912.

Harris, A., and Golding, S., 2002, New evidence of magmatic-fluid–related phyllic alteration: Implications for the genesis of porphyry Cu deposits: Geology, v. 30, p. 335–338.

Harris, A.C., Golding, S.D., and White, N.C, 2005, Bajo de la Alumbrera copper-gold deposit: Stable isotope evidence for a porphyry-related hydrothermal system dominated by magmatic aqueous fluids: Economic Geology, v. 100, p. 863–886.

Hedenquist, J.W., Matsuhisa, Y., Izawa, E., White., N., Giggenbach, W., and Aoki, M., 1994, Geology, geochemistry, and origin of high sulfidation Cu-Au mineralization in the Nansatsu district, Japan: Economic Geology, v. 89, p. 1–30.

Hedenquist, J., Arribas, A., and Reynolds, J., 1998, Evolution of an intrusion-centered hydrothermal system: Far Southesat-Lepanto porphyry and epithermal Cu-Au deposits, Philippines: Economic Geology, v. 93, p. 373–404.

Holland, T.J.B., and Powell, R., 1998, An internally consistent thermodynamic data set for phases of petrological interest: Journal of Metamorphic Geology, v. 16, p. 309–343.

Johnson, J., Oelkers, E., and Helgeson, H., 1992, SUPCRT92: A software package for calculating the standard molal thermodynamic properties of minerals, gases, aqueous species, and reactions from 1 to 5000 bar and 0 to 1000°C: Computers and Geosciences, v. 18, p. 899–947.

Manske, S., and Paul, A., 2002, Geology of a major new porphyry copper center in the Superior (Pioneer) district, Arizona: Economic Geology, v. 97, p. 197–220.

Masterman, G.J., Cooke, D.R., Berry, R.F., Walshe, J.L., Lee, A.W., and Clark, A.H., 2005, Fluid chemistry, structural setting, and emplacement history of the Rosario Cu-Mo porphyry and Cu-Ag-Au epithermal veins, Collahuasi district, northern Chile: Economic Geology, v. 100, p. 835–862.

Mercer, C., and Reed, M., 2013, Porphyry Cu-Mo stockwork formation by dynamic, transient hydrothermal pulses: Mineralogic insights from the deposit at Butte, Montana: Economic Geology, v. 108, p. 1347–1377.

Meyer, C., 1965, An early potassic type of wall rock alteration at Butte, Montana: American Mineralogist, v. 50, p. 1717–1722.

Meyer, C., and Hemley, J.J., 1967, Wall rock alteration, *in* Barnes, H.L. ed., Geochemistry of hydrothermal ore deposits: New York, Holt, Rinehart and Winston, Inc., p. 166–232.

Meyer, C., Shea, E., Goddard, C., and staff, 1968, Ore deposits at Butte, Montana, *in* Ridge, J.D. ed., Ore deposits of the United States 1933–1967, The Graton-Sales Volume: New York, American Institute of Mining, Metallurgical, and Petroleum Engineers, v. 2, p. 1363–1416.

Muntean, J.L., and Einaudi, M.T., 2001, Porphyry-epithermal transition: Maracunga belt, northern Chile: Economic Geology, v. 96, p. 743–772.

Ossandón, G., Fréraut, R., Gustafson, L.B., Lindsay, D.D., and Zentilli, M., 2001, Geology of the Chuquicamata mine: A progress report: Economic Geology, v. 96, p. 249–270.

Page, R.H., 1979, Alteration-mineralization history of the Butte, Montana ore deposit, and transmission electron microscopy of phyllosilicate alteration phases: Unpublished Ph.D. thesis, Berkeley, CA, University of California, Berkeley.

Proffett, Jr., J.M., 1979, Ore deposits of the western United States—a summary, *in* Ridge, J.D., ed., Papers on mineral deposits of western North America—the International Association on the Genesis of Ore Deposits Fifth Quadrennial Symposium: Nevada Bureau of Mines and Geology Report 33, p. 13–32.

Reed, M.H., 1979, Butte district early stage geology synthesis: Unpublished Anaconda Company Report, 42 p.

——1980, Distribution of mineralization at Butte, an addendum: Unpublished Anaconda Company Report, 25 p.

——1981, Summary of recent developments in the interpretation of Butte geology: Unpublished Anaconda Company Report, 28 p.

——1997, Hydrothermal alteration and its relationship to ore fluid composition, *in* Barnes, H.L., ed., Geochemistry of hydrothermal ore deposits, 3rd edition: New York, John Wiley & Sons, p. 303–366.

——1998, Calculation of simultaneous chemical equilibria in aqueous-mineral-gas systems and its application to modeling hydrothermal processes: Reviews in Economic Geology, v. 10, p. 109–124.

Reed, M., and Palandri, J., 2006, Sulfide mineral precipitation from hydrothermal fluids: Reviews in Mineralogy and Geochemistry, v. 61, p. 609–632.

——2010a, SOLTHERM.XPT, a database of equilibrium constants for minerals and aqueous species: Eugene, Oregon, University of Oregon, available from the authors.

——2010b, Ascent and cooling of magmatic fluids: Precipitation of vein and alteration minerals, *in* Birkle, P., and Torres-Alvarado, I., eds., Water-rock interaction: London, CRC Press, Taylor and Francis Group, p. 37–40.

Roberts, S.A., 1973, Pervasive early alteration in the Butte district, Montana, *in* Miller, R.N., ed., Guidebook for the Butte field meeting of Society of Economic Geologists: Butte, The Anaconda Company, p. HH1–HH8.

——1975, Early hydrothermal alteration and mineralization in the Butte district, Montana: Unpublished Ph.D. dissertation, Cambridge, MA, Harvard University, 157 p.

Rusk, B.G., and Reed, M.H., 2002, Scanning electron microscope-cathodoluminescence analysis of quartz reveals complex growth histories in veins from the Butte porphyry copper deposit, Montana: Geology, v. 30, p. 727–730.

Rusk, B., Reed, M., Dilles, J.H., Klemm, L., and Heinrich, C.A., 2004, Compositions of magmatic hydrothermal fluids determined by LA-ICP-MS of fluid inclusions from the porphyry copper-molybdenum deposit at Butte, Montana: Chemical Geology, v. 210, p. 173–199.

Rusk, B., Reed, M., and Dilles, J., 2008a, Fluid inclusion evidence for magmatic-hydrothermal fluid evolution in the porphyry copper-molybdenum deposit at Butte, Montana: Economic Geology, v. 103, p. 307–334.

Rusk, B.G., Miller, B.J., and Reed, M.H., 2008b, Fluid inclusion evidence for the formation of main stage polymetallic base-metal veins, Butte, Montana, USA: Tucson, Arizona Geological Society Digest, v. 22, p. 573–581.

Sales, R.H., 1914, Ore deposits at Butte, Montana: Transactions of the American Institute of Mining, Metallurgical and Petroleum Engineers, v. 46, p. 3–109.

Sales, R., and Meyer, C., 1948, Wall rock alteration at Butte: American Institute of Mining and Metallurgical Engineers, Transactions, v. 46, p. 4–106.

Saunders, J., Hofstra, A., Goldfarb, R., and Reed, M., 2013, Geochemistry of hydrothermal gold deposits, *in* Scott, S., ed., Geochemistry of mineral deposits, treatise on geochemistry II: Amsterdam, Elsevier, in press.

Seedorff, E., and Einaudi, M., 2004a, Henderson porphyry molybdenum system, Colorado: I. Sequence and abundance of hydrothermal mineral assemblages, flow paths of evolving fluids, and evolutionary style: Economic Geology, v. 99, p. 3–37.

——2004b, Henderson porphyry molybdenum system, Colorado: II Decoupling of introduction and deposition of metals during geochemical evolution of hydrothermal fluids: Economic Geology, v. 99, p. 39–72.

Seedorff, E., Dilles, J.H., Proffett, J.M., Einaudi, M.T., Zurcher, L., Stavast, W.J.A., Johnson, D.A., and Barton, M.D., 2005, Porphyry deposits: Characteristics and origin of hypogene features: Economic Geology 100th Anniversary Volume, p. 251–298.

Shock, E.L., and Helgeson, H.C., 1988, Calculation of the thermodynamic and transport properties of aqueous species at high pressures and temperatures: Correlation algorithms for ionic species and equation of state predictions to 5 Kb and 1000°C: Geochimica et Cosmochimica Acta, v. 52, p. 2009–2036.

Shock, E.L., Sassini, D.C., Willis, M., and Sverjensky, D.A., 1997, Inorganic species in geologic fluids: Correlations among standard molal thermodynamic properties of aqueous ions and hydroxide complexes: Geochimica et Cosmochimica Acta, v. 61, p. 907–950.

Sillitoe, R.H., 2010, Porphyry copper systems: Economic Geology, v. 105, p. 3–41.

Smedes, H.W., 1973, Regional setting and general geology of the Boulder batholith, Montana, in Miller, R.N., Guidebook for the Butte field meeting of the Society of Economic Geologists: Butte, Montana, Anaconda Company, p. A1–A6.

Snee, L., Miggins, D., Geissman, J., Reed, M., Dilles, J., and Zhang, L., 1999, Thermal history of the Butte porphyry system, Montana [abs.]: Geological Society of America Abstracts with Program, v. 31, p. 380.

Spear, F.S., 1993, Metamorphic phase equilibria and pressure-temperature-time paths: Washington, D.C., Mineralogical Society of America Monograph, 799 p.

Spycher, N.F., and Reed, M.H., 1989, Evolution of a Broadlands-type epithermal ore fluid along alternative P-T paths: Implications for the transport and deposition of base, precious, and volatile metals: Economic Geology, v. 84, p. 328–359.

Stoffregen, R., 1987, Genesis of acid-sulfate alteration and Au-Cu-Ag mineralization at Summitville, Colorado: Economic Geology, v. 82, p. 1575–1591.

Streckeisen, A., 1974, Classification and nomenclature of plutonic rocks recommendations of the IUGS Subcommission on the Systematics of Igneous Rocks: Geologische Rundschau, v. 63, p. 773–786.

Tilling, R.I., 1973, The Boulder batholith, Montana: Product of two contemporaneous but chemically and isotopically distinct magma series, in Miller, R.N., ed., Guidebook for the Butte field meeting of the Society of Economic Geologists: Butte, Montana, Anaconda Company, p. Cl–C5.

Watanabe, Y., and Hedenquist, J.W., 2001, Mineralogic and stable isotope zonation at the surface over the El Salvador porphyry copper deposit, Chile: Economic Geology, v. 96, p. 1775–1797.

Weed, W.H., 1912, Geology and ore deposits of the Butte district, Montana: USGS Professional Paper 74, 262 p.

Zhang, L., 2000, Stable isotope investigation of a hydrothermal alteration system; Butte porphyry copper deposit: Unpublished Ph.D. dissertation, Corvallis, Oregon, Oregon State University, 182 p.